Article

Development of a GIS Tool for a High Precision PV Degradation Monitoring and Supervision: Feasibility Analysis in Large and Small PV Plants

Miguel De Simón-Martín [1],*, Ana-María Diez-Suárez [1], Laura Álvarez-de Prado [2], Alberto González-Martínez [1], Álvaro De La Puente-Gil [1] and Jorge Blanes-Peiró [1]

[1] Department Area of Electrical Engineering, University of León (Spain), School of Mines Engineering, Campus de Vegazana s/n, 24071 León, Spain; ana.diez.suarez@unileon.es (A.-M.D.-S.); alberto.gonzalez@unileon.es (A.G.M.); apueng01@estudiantes.unileon.es (Á.D.L.P.-G.); jorge.blanes@unileon.es (J.B.-P.)

[2] Department Area of Topography, University of León (Spain), School of Mines Engineering, Campus de Vegazana s/n, 24071 León, Spain; laura.alvarez@unileon.es

* Correspondence: miguel.simon@unileon.es; Tel.: +34-987 29 10 00 - 5391.

Abstract: It is well known that working PV plants show several maintenance needs due to wiring and modules degradation, mismatches, dust and PV cells defects and faults. There are a wide range of studies that show the theoretical and some laboratory tests of how these circumstances may affect the PV production. Thus, it results mandatory to evaluate the whole PV plant performance and, then, it's payback time, profitability and environmental impact or carbon footprint. However, very few studies include a systematic procedure to quantify and supervise the real degradation effects and faults impacts on the field. In this paper, the authors first conduct a brief review of the most frequent PV faults and degradation that can be found on real conditions operative PV Plants. Then, they propose and develop an innovative Geographic Information System application to locate and supervise them. The designed tool has been applied to either a large PV plant of 108 kWp and a small PV plant of just 9 kWp installed on a home rooftop. For the large PV plant, 24 strings of PV modules have been modelized and introduced into the GIS application and every module in the power plant has been studied including voltage, current, power, series and parallel resistance, fill factor, normalized PV curve to STC, thermography and visual analysis. For the small PV installation 3 strings of PV panels have been studied identically. It must be noticed that PV modules in this case include power optimizers. The precision of the study allows the researchers to locate and supervise up to a third part of every PV cell in the system, which are adequately georreferenciated. The developed tool allows both the researchers and the investors to increase control on the PV plant performance and conducts to a better planification of maintenance actuations and to evaluate several PV modules replacement strategies in a preventive maintenance programme. Found PV faults include hot spots, snail tracks, EVA discoloration, PV cells fractures, busbars discoloration, bubbles and Si discoloration.

Keywords: photovoltaics; PV plants; PV faults; Geographic Information System; PV supervision and maintenance

1. Introduction

The operation and maintenance of a photovoltaic (PV) power plant results of extreme importance to guarantee its optimal performance. In fact, monitoring is not just a regular recording of data but involves a more detailed analysis in order to prevent possible malfunctions witch its associated power and economic losses. However, most photovoltaic power plants just record few operative data in order to check a proper operation, but it is not usual that maintenance service carry out a detailed analysis. Effective maintenance involves at least semiautomatic analysis and alerts. In this way, the maintenance operator is allowed to make immediate decisions and solve safety problems and minimize power losses [1].

The main objective of this study is to design a tool that allows the maintenance service to carry out an effective supervision of the power plant and, what is more important, to monitor the evolution of the modules behavior in an easy and feasible way. In fact, automated monitoring of photovoltaic plants is becoming necessary to evaluate the aging of the panels and the early detection of operating failures. Thus, significantly much more effective management plans, preventive maintenance policies and early replacement of poor performance components can be carried out with successful results.

Accurate measurement, control and evaluation systems are fundamental for the main participant agents in the photovoltaic industry. For device manufacturers, the evaluation of the performance of their products is a reference of their quality manufacturing processes. On the other hand, researchers from companies can take advantage of them and use that information to identify future needs in the industry and test real working conditions. For PV plants promoters and owners, realistic performance data results essential for investment decision making.

The related literature shows several strategies based on physical modelling and polynomial regression between DC power estimations and real AC power production. Subsequently, these results are applied to the detection of real and/or potential failures on the PV field [2]. However, this sort of techniques is found to be limited in the sense they do not detect the existing anomaly (e.g. module failure, power production losses, safety dangers, etc.) until it occurs and consequences cannot be avoided. Furthermore, these techniques are not adequate to implement effective preventive maintenance strategies or carry out an economic and effective components replacement schedule.

Other monitoring approaches are based on performance indicators calculated through electro-thermal modelling techniques of the PV plant [3]. As these indicators are calculated on a daily basis, thus they are also not effective for our purposes.

On the other hand, the latest data acquisition systems that have been integrated on the supervision and monitoring devices for photovoltaic plants are based on wireless technology such as *Zigbee*, according to IEEE 802.15.4, based specification for personal area networks. Parameters such as temperature, irradiation, DC power input in the inverter and AC power output to the grid can be easily obtained. Furthermore, the acquired data can be uploaded to the cloud almost in real time and send notification alerts to the power plant owners and maintenance service [4]. However, these systems still do not integrate georeferences tools that may help to improve the application of a preventive maintenance strategy.

Our experience both in the laboratory and in the real field regarding PV power plants have conducted us to design a new methodology to locate and analyze malfunctions, faults and outrageous performances from the plant components in a global context. The analysis carried out in a laboratory result of high interest, but many times they do not result operative in the application of real maintenance plans. Although test conditions in laboratory allows a deep analysis of the PV components under study, it involves unaffordable costs for the owners and sometimes implies to put the complete or part of the installation out of order. Moreover, test conditions at the laboratory may not be representative of the real working conditions at the working field. Thus, the conclusions from laboratory test may be decontextualized. On the other hand, analysis techniques on field are influenced by the climatic and environmental conditions, that are not usually stable and to carry out a systematic procedure becomes not an easy task.

For this reason, a new methodology has been proposed combining the precision of standard laboratory tests and a feasible and effective maintenance procedure. The integration of Geographic

Information System (GIS) platforms suppose a significant advantage in the sense that all tests related information is adequately organized and georeferenciated. Thus, not only particular impacts of a defect on a single component can be studied, but its impact on the overall performance can be then analyzed. Then, predictive techniques that analyze variations on the behavior of apparently sane components can be applied and predict possible malfunctions on a certain zone of the power plant.

A properly developed GIS tool allows a comprehensive analysis of the territory with application to any activity that involves a spatial component. In this way, the GIS technology has a wide field of application in the management of resources. In addition, this is an essential tool in decision-making tasks where the spatial component has a certain relevance.

In the past decade several applications of the GIS tools to the Energy field have arisen, specially to locate energy resources, build solar atlas, etc. For example, Höhn et al. applied a GIS tool to analyze the spatial distribution of biomass resources in a certain region of Finland to optimize the location of biogas power plants [5]. On the other hand, other authors have taken advantage of GIS tools to create solar atlas and estimate with high precision the power potential of Concentrated Solar Energy (CSP) power plants [6].

Also in the field of photovoltaic energy, the application of GIS techniques is an innovative approach that has taken a quick relevance, especially in the design, management and supervision of large PV power plants. Thus, just to cite some examples, Kakumoto et al. presents a GIS based technique to estimate PV production taken into account with precission the shadowing effect [7]; and Tsanakas et al., by the combination of the aerial triangulation techniques and the terrestrial georeferentiation, propose a technique to create virtual dynamic maps of a power plant, including georeferenciated thermal images [8]. Other authors have used GIS together with Global Positioning Systems (GPS) and Unmanned Aerial Vehicles (UAV) to propose an efficient inspection and maintenance of PV plants [9].

According to these examples, the potential of the utilization of GIS based methodologies in the energetic field seems to be of great interest in the near future.

The purpose of this work is to extend the application of the GIS tools in the photovoltaic field, not only to the resource location, but in the operation and maintenance of PV power plants as well. This is really of interest in large plants. Early fault detection may result in a significant improvement of the power plant performance, and the inclusion of spatial information is a novel approach that may lead to new predictive and preventive maintenance programs.

This study aims to evaluate the potential of a specifically designed GIS tool in the location of PV faults and analysis of the degradation effects on PV power plants working in real operation conditions. As cases study, the proposed tool has been applied to two representative PV plants: a 108 kW peak power (kWp) grid connected power plant and a 9 kWp self-consumption power plant.

The most commonly spread real degradation effects and faults impacts on the field, observable or measurable, that affect or may affect the future production of energy of the photovoltaic plants have been included in the analysis. Only faults on the PV modules have been included. Wiring degradation, inverter faults, aging and other electrical and mechanical malfunctions have been excluded from the preliminary version of the developed tool, although they may be included in future versions.

This article is organized in five sections. First, a brief review of the most common PV faults is exposed. Then, the methodology and the tool characteristics are described. In section 4, the application of the developed tool is exposed and two representative cases study are fully described including the results discussion of the developed GIS tool implementation. Finally, last section includes the main conclusions and future research directions.

2. State of the art of PV modules defects

The literature defines a failure in a photovoltaic module as an effect that degrades the module power output which is not reversed by normal operation or, on the other hand creates a safety issue. Sometimes, both effects can occur simultaneously. A purely aesthetic problem is, then, not considered

as a failure of the PV module. Wiring and modules degradation, mismatches, dust and PV cells defects and faults, are considered as failures of PV modules [10].

A systematic review has been conducted in order to show the state of the art in this field with precision. According to Urra Medina et al., a systematic review is defined as a process to identify the core of a narrative review which may result worth of interest in practice [11]. In this case, the identification of the review purpose answers the question *"which PV faults are the most representative in the literature and may affect more significantly to the power production of a PV plant?"*. This research question, as required in the systematic review methodology, is delimited, accessible and distinguishable in the literature [12]. Thus, the following bound conditions for the review have been applied:

- **Sources:** only papers from indexed international journals, scientific books edited by international editors, international conference proceedings, technical review reports from prestigious international organizations and open access Ph.D. Thesis have been included in the research.
- **Language:** English and Spanish.
- **Publication period:** only research works published in the period from 2000 to 2016 have been considered.
- **Requirements:** selected contributions must be open access or available in international databases, peer-reviewed and guarantee traceability in the research.
- **Type:** both original research contributions and review works have been included in the analysis.

Once the searching criteria were defined, the literature review was conducted and results can be seen in Table 1, where the most common defects have been identified and classified. It must be notice that books and Ph.D. Thesis have been grouped, as well as review works and technical reports. Results show 5321 references, where the 66% are journal articles and 25% are books and Ph.D. Thesis.

Figure 1 shows examples of several of the described defects. Following subsections describe briefly all found PV modules potential failures.

Table 1 – Systematic review on PV defects results. Number of references.

| Failures	Conference papers	Journal Articles	Articles in press	Reviews and Reports	Books and Ph.D. Thesis
Delamination	58	37	2	2	2
Adhesion loss from the backsheet films	4	65	0	2	11
Faults in the junction box	1	249	0	9	145
Frame breakages	2	228	0	9	122
EVA discoloration	9	28	1		4
Bubbles formation	3	237	0	10	89
Cell cracks	9	357	0	27	221
Snail tracks	6	34	0	2	13
Burn marks	0	473	0	21	264
Potential induced degradation	173	953	0	38	67
Disconnected cells and string interconnected ribbons	3	29	0	0	41
Defective by-pass diode	1	197	0	4	82
Hot spots on cells	11	636	2	34	294
TOTAL	**280**	**3523**	**5**	**158**	**1355**
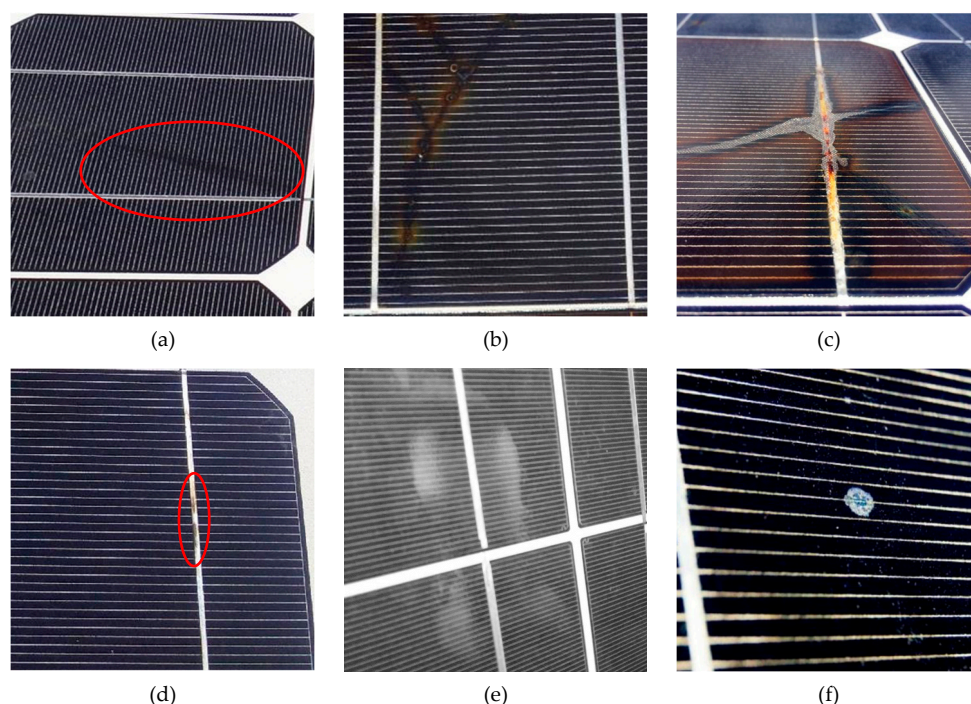
Figure 1 – Defects identification examples. (a) Snail track. (b) Cell crack. (c) Hot spot. (d) Busbar discoloration. (e) EVA discoloration. (f) Bubble formation.

2.1. Delamination

The adhesion between the glass, encapsulation, active layers and the back layers can be compromised for various reasons. Larger thin film modules and some other type of technology may also contain a transparent conductive oxide (TCO) layer from the soda-lime glass substrate. This layer may lose adhesion with the adjacent glass layer [13]. Usually, if adherence is compromised due to contamination (e.g. by inadequate cleaning of the glass) or environmental factors, delamination will occur, followed by moisture formation and, thus, corrosion. The delamination of the interfaces that are within the optical path of the light, will give rise to a reflection and the consequent loss of current (power) on the modules.

Delamination can be relatively easy to detect by visual inspection. The detachment of the layers can be quantified using a reflectometer. On the other hand, there are delaminations that cannot be visually identified and therefore, other methods must be used, such as pulsed active thermography or *"lock-in"* thermography. X-ray tomography and the ultrasound scanner are used to examine smaller delaminations. This way, a much higher resolution can be get, but both methods require a longer evaluation time [14].

2.2. Adhesion loss of the backsheet films

The most backsheet films for PV modules are multilayer composites comprising three or more polymer layers. The outer layers have to be resistant against various weathering impact factors (e.g. irradiance, humidity…). Often used protection layers are fluoropolymers, such as the polyvinylfluoride (PVF), the polyamide (PA) or the polyethylene terephthalate (PET) [15].

Reported failures of backsheets are delamination within the multilayer laminate, embrittlement leading to cracks or yellowing. The worst failures within backsheets are cracks and delaminations, as they allow enhanced water vapor and oxygen ingress into the PV module and can cause safety problems due to the loss in the isolation properties [16]. Water vapor is known to have a critical impact on various degradation phenomena like corrosion of the metallic parts, potential induced degradation (PID) of PV modules and encapsulate decomposition. Therefore, these failure modes can reduce the performance of a PV module and shorten its lifetime. However, the yellowing effect, is reported to have no influence on the electrical performance of the modules.

2.3. Mechanical breakage and junction box faults

Mechanical breakages are usually identified as frame cracks produced due to poor handling conditions or extreme snow loads in winter.

The junction box is the container, attached to the back of the module, which protects the connection of the strings of the module to the external terminals. Usually, the junction box contains the bypass diodes, which protect the cells of a series in case hot spots are produced mainly due to partial shadowing of the module [10]. It has been reported in the field faults in the adhesive system, and overtures on the junction box that provoke moisture formation and, then, wiring degradation. This type of failures affects mainly to the safety, being able to produce an electric arc and even fire danger.

2.4. Encapsulation discoloration and bubbles formation

The encapsulation material (usually, Ethylene Vinyl Acetate or EVA) degradation is an aesthetic issue that usually does not affect the module's performance. However, this degradation may conduct to a current loss with an average of 0.5%/year and a median of 0.8%/year for a Si PV module [17].

On the other hand, bubbles are generally caused by the evolution of gas elements directly or indirectly during melt and solidification procedures, because in the manufacturing process the photovoltaic module, is exposure to inappropriate temperatures or excessively long periods during the lamination process [18].

2.5. Cell cracks

PV cells are made of silicon so they are very brittle. Cell cracks are formed in different lengths and orientations in the substrate of the photovoltaic cells and, often, cannot be easily seen. Cell cracks can be caused during cell production or after finishing the production. The major sources for cell cracks are the packaging/transport and reloading of PV modules and the installation process in the field.

Once cell cracks are present in a solar module, there is an increased risk that during operation of the solar module short cell cracks can develop into longer and wider cracks. This is because of mechanical stress [19] caused by wind or snow load and thermo-mechanical stress [20] on the solar modules due to temperature variations caused by passing clouds and variations in weather.

Therefore, an inactive cell area of more than 8% is not acceptable. Besides the risk of power loss there is a chance of hot spots due to inactive cell parts greater than 8%. This happens if the cracked cell has a localized reverse current path in the still active cell part. Due to the missing cell area the cell is driven into reverse bias and the full current can flow along the localized path. This may cause hot spots and therewith burn marks [21].

2.6. Snail tracks

Snail tracks are discolorations of the silver fingers on solar cells. In the PV module the effect looks like a snail track on the front glass of the module. The discoloration occurs at the edge of the solar cell and on not visible cell cracks. The discoloration typically occurs between 3 months to 1 year after installation of the PV modules [22]. The initial discoloration speed depends on the season and the environmental conditions. During the summer and in hot climates, snail tracks seem to spread faster [10]. In [23], the authors compare the results of the PV modules affected by the snail track with a reference module under laboratory conditions. The results showed that the maximum power under standard conditions is reduced by 40%, and the energy production measured over 30 days was approximately 25% lower than expected.

2.7. Burn marks and hot spots

One of the most common and typical failures in silicon modules are burn marks. This failure is associated with parts of the module that become very hot because of solder bond failure, ribbon

breakage, localized heating from application of reverse current flow or other hot spots [10]. Burn marks produce unquantified power losses and safety problems.

A hot spot is a phenomenon that defines a region located in a photovoltaic module whose operating temperature is very high compared to the surrounding regions. This can happen when a cell generates less current than the rest of the cells connected in series as a consequence of [24]:

- Partial shading.
- Potential-induced polarization with respect to ground in modules manufactured with novel techniques (voltage, both positive and negative, depending on the type of cell considered).
- Intrinsic defects in the cell.
- Dispersion of characteristics between modules of a generator and between cells of the same module connected in series.
- Interconnection failure.

As a result, the defective cell is polarized, (the voltage between the positive and negative terminals becomes negative), and behaves as a charge dissipating in heat the power generated by the rest of the series cells.

2.8. Potential induced degradation

The potential induced degradation causes power losses due to the presence of eddy currents in the PV modules. Its potential effect can reduce the power of the equipment [25].

The reported main cause of these currents is the presence of voltages gaps between the module and the ground. In most photovoltaic systems without a grounding system, the modules have a non-zero voltage that provokes this effect. Negative voltages are more frequently reported, especially under high voltage conditions, high ambient humidity and/or high ambient temperatures [26].

2.9. Disconnected cells and string interconnected ribbons.

Cell strings are disconnected due to the weakness of the string interconnected ribbons. Main causes of this effect are poor quality welds in the PV module production process, weak connections between the cells ribbon and the string or deep deformations. Moreover, a narrow distance between the cells promotes the cell interconnected ribbon breakage. [10].

Likewise, there may be multiple consequences: shunt by cell interconnected ribbon with reduction of open circuit voltage, broken cell interconnected ribbon with reduction of maximum power point current [27].

2.10. Defective by-pass diode.

By-pass diodes are used to minimize the effects of partial shading on the PV module power generation. By-pass diodes are required to limit the potential of a reverse voltage produced because partial shading [10].

Without by-pass diodes, partial shading on photovoltaic solar cells reduce dramatically its power output and can cause local overheating leading to severe damages [28].

3. Materials and Methods

In this section, the innovative developed GIS tool will be described first. Then, the measurement process and used equipment will be detailed. All measurements have been taken according to the adequate standards with the minimum uncertainties affordable using on field working equipment.

3.1. GIS tool implementation

A GIS is a set of programs and computer applications that allow the management of data organized in databases, referenced spatially and visualized through maps [29]. Thus, it is a powerful

analysis tool that can include spatial and/or geographical data -referenced to a map- although they can also include non-spatial data.

The proposed tool in this study aims to collect and compile a dataset of several PV power generation variable values into a GIS tool in order to easily visualize and locate problems in a PV power plant and to predict its spread. Thus, a base map and an associated database have been created, as well as the proper procedures to systemize the data introduction and analysis. In this way, the study of the evolution of existing defects, including electrical and thermal parameters, becomes simpler. Moreover, as novel approach, the developed tool allows to correlate the PV defects existence not only with power losses on the affected PV module, but to the overall performance of the PV power plant.

The complete PV power plant was first introduced into the GIS software (ESRI ArcGIS) by aerial ortophotographs and project geometrical parameters. Thus, the limits of the plots and the geographical position of the PV series strings organization were set. Figure 2 shows both the representation of the analyzed PV plant and the division into strings.

Furthermore, it is mandatory to identify the exact position within the panel of the possible faults. For this reason, it was taken into account the split installation with photovoltaic panels and the thirds of cell within each panel. This means that the 60 solar cells of each panel are divided into 3 parts, thus each photovoltaic module is formed by 180 thirds of cells. The maps have been georeferenced by assigning them projected coordinates ETRS89 UTM 30N.
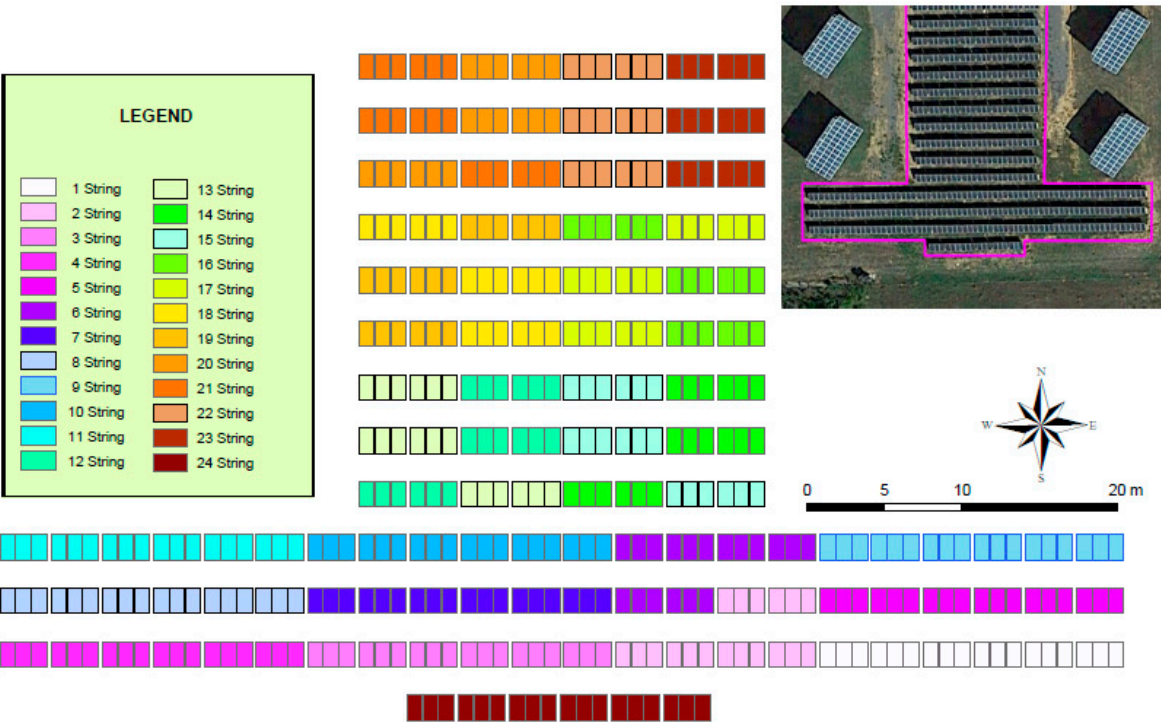

Figure 2 - Aerial photograph and string distribution of the 108 kWp PV plant implemented.

As seen in Figure 2, the reference of the position of the modules within the string series begins in the low left corner in the map. Then, each PV module, in addition to be identified with the rack number, it can also be identified with a simple code which includes the series string and the relative position within the string series.

A systematic procedure must be established to identify the geographical position of the defect within the panel. As each photovoltaic module consists of 180 thirds of cells, the following nomenclature was proposed. Each cell in the solar panel is divided into 10 rows (0-9) and 6 columns (A-F). In turn, each cell has been divided into 3 thirds (X, Y or Z), depending on their position. Therefore, when indicating the position of a defect, the third of cell where it is located within the

panel can be identified by a three alphanumerical symbols code (e.g. 2CY). Figure 3 shows the adopted identification system on a panel.
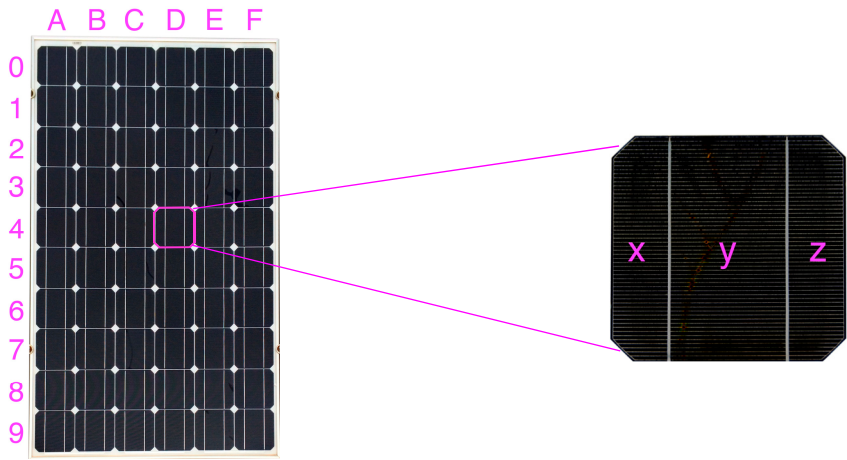

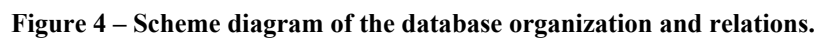**Figure 3 – Adopted nomenclature for a PV defect identification.**

Once the graphical part of the GIS tool has been defined and the identification procedure for each component has been established, a georeferenced database (geodatabase) has been implemented. The geodatabase is a set of several types of geographic datasets embedded in a common file system folder. In our case, a geodatabase has been particularly created that has a comprehensive information model to represent and manage geographic information related to a PV power plant. This comprehensive information model is implemented as a series of tables that store entity classes, raster datasets, and attributes.

The designed information model is divided into three sorts of information: electrical variables measures, graphic information (pictures and thermographies) and defects existence and description. Figure 4 shows the scheme diagram of the relational database. According to the three sorts of information, it has been organized into four main tables and four auxiliary tables.

The first main table, named PV MODULES, includes all the information related to the analyzed PV module, including an identifier code (ID_MOD) which is the Primary Key of the table (identifies uniquely each record), the associated inverter (INVERTER), the string series (SERIES), the relative position in the series (POSITION IN SERIES), the rack number (RACK NUMBER) and its manufacturing reference code (PV MODULE REFERENCE NUMBER).

The table named MEASUREMENTS includes all the measured electrical variables that will allow the performance analysis. It assigns to each measurement a unique identifier (ID_MEASURE) and relates each measurement record to the PV module through the ID_MOD. It also includes the date when the measurement was taken (DATE) and the inspector who did it (INSPECTOR). The factory settings where introduced into the database setting INSPECTOR as *"FACTORY"* and as date the installation date. Moreover, in order to guarantee a proper analysis, the measurement quality (metadata) has been included in other parameter named MEASURE QUALITY, which is an 8 digits' code described in the auxiliary table named QUALITY.

The quality code is a metadata field which gives information about the stored data. It is a number between 0 and 9 that can take the following values: 0: the record is a calibration value, 1: the record has no validation, 2: the record has been checked to be in range, 3: the record has passed the time coherence test (assigned timestamp is correct), 4: the record has passed the internal coherence test, 5: the record has passed the time series coherence test, 6: the record has passed the spatial coherence test, 7: the record is considered not valid because external disturbances, 8: the measure was not recorded and 9: the measure was not directly measured (it was interpolated or calculated from others). There exists one digit for each electrical measured value.

Figure 4 – Scheme diagram of the database organization and relations.

PV defects and faults have been introduced in the DEFECTS table. Each record identifies the affected module (ID_MOD), the cell through the location code (CELL), the affected third of cell (POSITION IN CELL) as well as the date (DATE), inspector (INSPECTOR), type of defect (TYPE) and evolution of the defect in the module (EVOLUTION).

Type value is an identifier described in the auxiliary table named DEFECT TYPE. PV faults were coded in the form 0: snail track, 1: cell crack, 2: hot spot, 3: busbar discoloration, 4: cell discoloration, 5: EVA discoloration, 6: blue cell and 7: other.

On the other hand, the EVOLUTION field in the DEFECTS table is associated to the auxiliary table named EVOLUTION. The evolution of the defect in the PV module is included according to the following descriptions 0: new defect or not detected before, 1: already detected but remains equal that on the previous inspection, 2: has increased from the previous inspection and 3: has decreased from the previous inspection.

Finally, graphic information can be also included. In this case, front and rear pictures of each analyzed module and front and rear thermographies has been taken. Moreover, the I-V curve obtained by a PV curve tracer has been stored. This information is organized in the FIGURES table which includes a hyperlink to the file (FILE), the type of figure (TYPE OF FIGURE) and its quality (FIGURE QUALITY). The type of figure is related to the auxiliary table named TYPE OF FIGURE. The figure quality is especially relevant in the case of thermographies and it is a one-digit code which description can be found in the previously described auxiliary table named QUALITY.

As it can be seen in Figure 5, both pictures, thermographies and I-V curves are associated and spatially referenced to each of the modules. This results very useful as it allows spatially relating the measured attributes in each panel with this graphical information. Moreover, all graphics are available not only from the geodatabase but for quick access through the GIS map.

Once the electrical measurements, faults detection and graphical information have been obtained, all data was compiled into a complete project constituting a GIS.

3.2. Measurement procedures and equipment

The followed methodology for the PV power plant status monitoring includes a visual and a measurement inspection. The visual inspection includes taking pictures of the front and rear parts of the PV module, as well as both calibrated thermographies. The measurement inspection involves the characterization of the PV module performance by the measurement of its characteristic I-V curve at working conditions and its extrapolation to the standardized STC conditions (incident global irradiance of 1000 W/m^2, cell temperature of 25°C and 1.5 air mass).

For the analysis of the thermal distribution in the PV modules a Fluke Ti40 thermal camera was used. It is mandatory to guarantee that there are no shadows on the PV modules during the process.

This could cause unexpected irregular thermal areas conducting to a misinterpretation of the results. Moreover, high wind speed conditions must be avoided as convection thermal exchange may diffuse the thermal image.
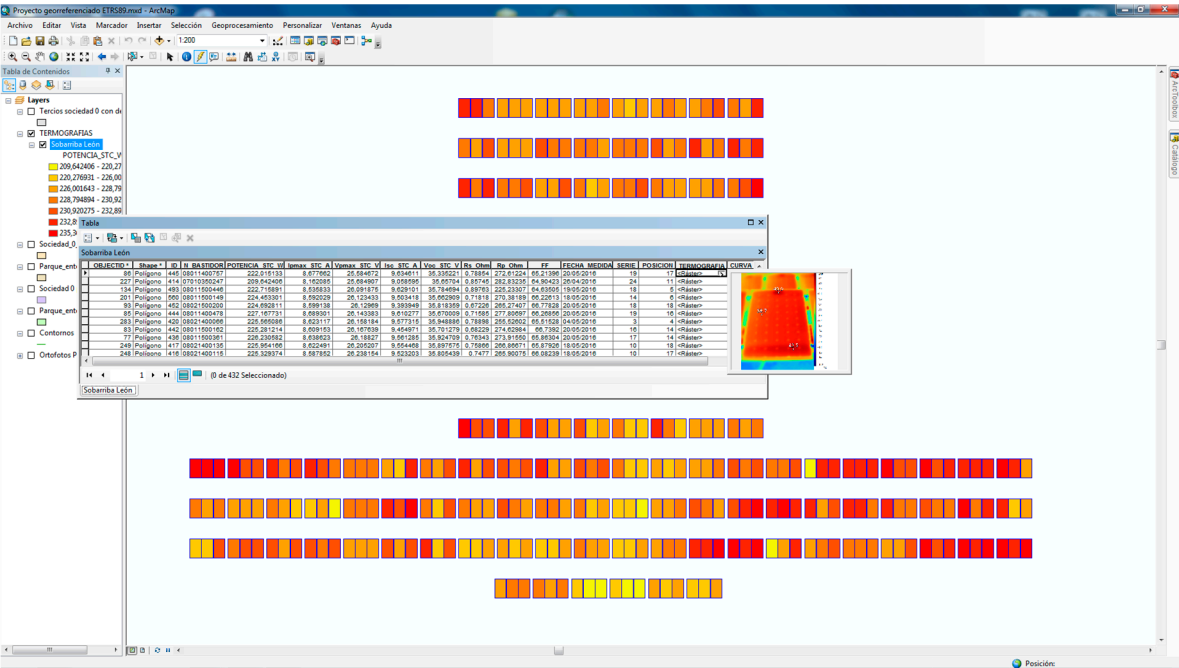

Figure 5 – Instantaneous access to a PV module frontal thermography.

The most favorable conditions to take a good quality and representative thermal image occurs when the panel is working at its maximum power conditions, which usually takes place with clear sky conditions at noon [30]. Thus, thermographies have been obtained only with minimum 700 W/m^2 of global irradiance on the horizontal surface and have been taken in the interval since 11 h to 13 h solar time. Moreover, in order to minimize interferences on the measure caused by reflections on the front part of the PV module, frontal and rear thermographies have been taken. However, special care on the corrections is needed for rear thermographies as temperature might be higher because there is no thermal dissipation as in the front part because of the cover glass [31]. Figure 6 shows both examples of thermographies taken from the frontal and the rear part of PV modules respectively.

(a)   (b)
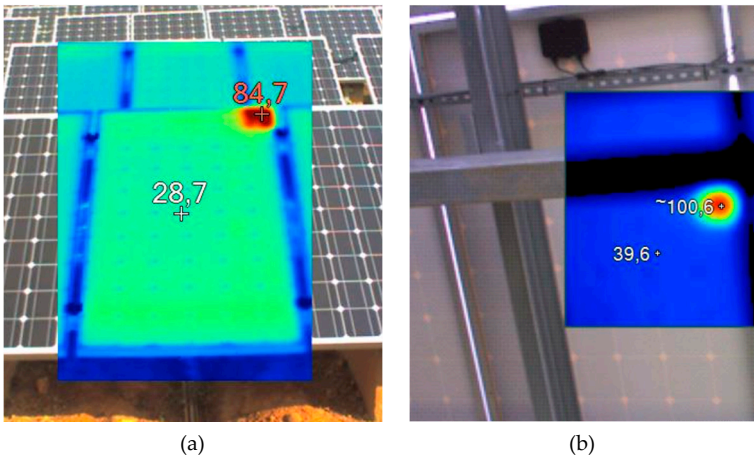
Figure 6 - Hot spot detection in (a) frontal and (b) rear taken thermographies.

The thermographic camera requires some parameters adjustment for the correct interpretation of the measured temperature: the emissivity (ε) and the background temperature (T_b). The emissivity varies depending on the surface, the ambient temperature and the radiation wavelength. In this case,

according to the literature, ε = 0.90 value has been set as reference for the front glass of the photovoltaic panel, whether ε = 0.86 was set for the rear thermographies pointing the Tedlar backsheet [32]. On the other hand, the background temperature refers to the surroundings of the measured surface and thus, the ambient temperature recorded from the facilities' weather station was set.

The measurement of the electrical parameters has been done with a PV curve tracer brand PVPM1000CX PVE with a NES Solar Radiation Sensor type SOZ-03 calibrated by a First Class pyranometer according to the WMO proposed methodology. The irradiance sensor includes an optimal temperature probe Pt100 mounted direct at the back side of the silicon cell of the SOZ-03 with an accuracy according to DIN EN 60751 Class A (±(0.15°C+0.002·T)). Moreover, an external temperature sensor Pt100 measures the PV module temperature for the STC correction. This device fulfils the international standard IEC 60904-1 (monocrystalline silicon) [33] and has an accuracy of the a/d converter of 0.25%, a peak power measurement uncertainty of ±5% and a reproducement of ±2%. The time taken to perform a single measurement with the device is comprised between 20 ms up to 2 seconds, avoiding the influence of capacitive properties of the module under test and minimizing measurement variations due to unstable weather conditions. Moreover, the PVPM measurement range is 0-1000 V and 0-20 A, that allows string measurements and checks. Thus, applying the algorithm described in [34,35] the STC *I-V* curve is obtained. Furthermore, all measurements have been taken with global irradiance on the generator plane greater than 800 W/m² and deviations lower than 1%. Both the device and an obtained measurement (*I-V* curve) can be seen in Figure 7.

(a)   (b)
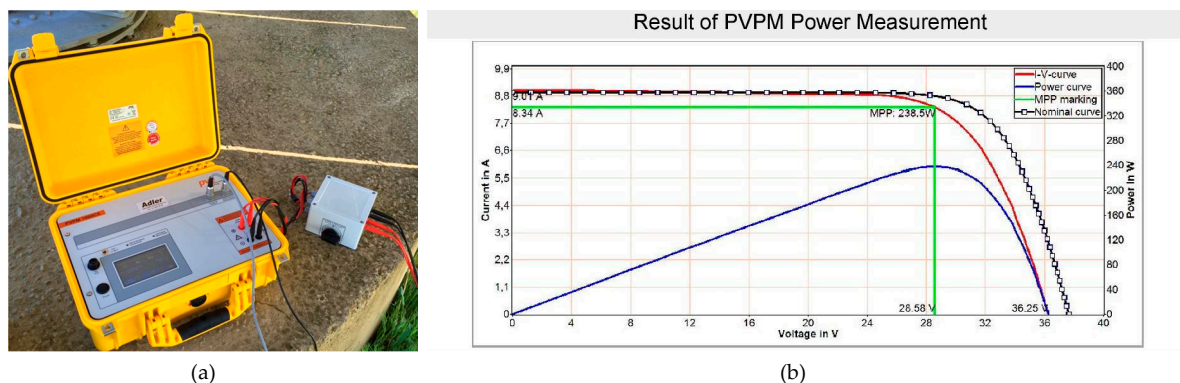
Figure 7 – I-V curve measurement. (a) PVPM1000CX curve tracer. (b) I-V curve example.

With the described device, short circuit current (*Isc*), open circuit voltage (*Voc*), maximum power point current (*Impp*) and maximum power point voltage (*Vmpp*), can be obtained with a measuring error <1%.

The internal series resistance (*Rs*) is calculated with a single measured *I-V* curve and a simulated one considering the fill factor (*FF*) is the same for both characteristics [36] and then applied the IEC 60891 procedure [37,38]. Using a simulated *I-V* curve prevents the variation of the *Rs* calculation due to the temperature, which has been stated in [39]. Nevertheless, even considering the influence of a slight temperature variation and the noise present in the *I-V* curve, the overall uncertainty for the determination of the series resistance is deduced to be ±10% and a repeatability of typically 5% [39].

On the other hand, the parallel resistance (*Rp*) is calculated as the inverse of the slope of the characteristic *I-V* curve in short circuit conditions. Thus, a linearization in the range between *Isc* and *a·(Isc-Impp)* was carried out, where *a* was optimized by an iterative numerical algorithm minimizing the variation of the *Rp* result. The evaluation of the accuracy of this method is not as simple as for *Rs* because the calculation procedure uses a numerical routine. Nevertheless, the obtained results are inside the tolerance of the values obtained for the *Rs*.

For high accuracy determination of the fill factor, Green provides approximate expressions for arbitrary shunt (parallel) and series resistances [40].

Table 2 shows the maximum measurement uncertainties for all measured electrical parameters expressed as percentage of the measured nominal value.

Table 2 – Maximum measurement uncertainties for the electrical parameters.

Measured parameter	Max. uncertainty [%]
STC Peak Power [W]	±5%
STC I_{mpp} [A]	±1%
STC V_{mpp} [V]	±1%
STC I_{sc} [A]	±1%
STC V_{oc} [V]	±1%
R_s [Ohm]	±10%
R_p [Ohm]	±10%
FF [%]	±2%

4. Results and discussion

The developed GIS tool has been applied to two cases study in Spain. The first one is a fixed 108 kWp PV plant connected to the grid, operating since mid-2008. The second one is self- consumption fixed domestic 9 kWp PV plant installed in the rooftop of a single family dwelling. This installation is in operation since February 2017.

4.1. Implementation on a 108 kWp PV power plant

This plant is operated by the Spanish company *Sobarriba Leon 0*, and it is characterized by 100 kW nominal power on the inverters and 108 kWp of installed PV modules. It constitutes part of a greater PV plant of 1 MW. Thus, it shares a transformation center formed by two 630 kVA transformers.

In this case, the PV modules are installed on fixed structures, pointing the South direction and tilted 28 degrees with the horizontal surface. The structures are made of steel and foundations are of concrete.

The PV field in this case consists of 432 *GFM 220-250* monocrystalline silicon modules 250 Wp manufactured by the company *Wuxi Guofei Green Energy Source Co. Ltd*. Their nominal electrical characteristics according to the manufacturer can be seen in table 3. They are organized in 24 strings (see Figure 2) with 18 modules on each, grouped in parallel through string electrical protection boxes. There are 6 string electrical protection boxes in total. All modules are fitted with adequate fuse protections.

Therefore, the inverter arrives 24 strings of 18 photovoltaic modules. The selected inverter is an *Ingecon Sun Power* model, manufactured by *Ingeteam*, and 100 kW nominal power. The inverter includes surge protection, a galvanic isolation transformer, DC fuses, anti-island with automatic disconnection protections, a thermal breaker, a reverse polarity protection, a protection against short-circuits and a protection against insulation faults.

Table 3 – Wuxi Guofei Green Energy GFM 220-250 PV module characteristics.

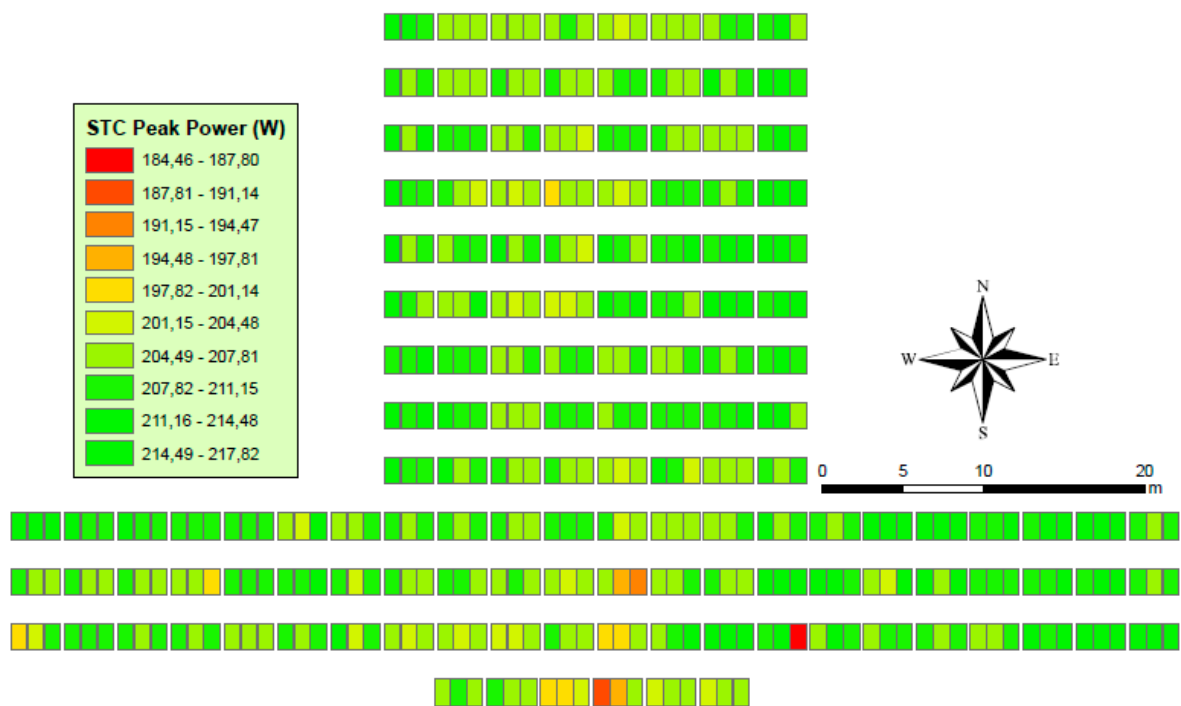| STC Peak Power [W]	STC I_{mpp} [A]	STC V_{mpp} [V]	STC I_{sc} [A]	STC V_{oc} [V]	*FF* [%]
250 ± 5%	7.96	31.4	8.38	37.2	0.8018

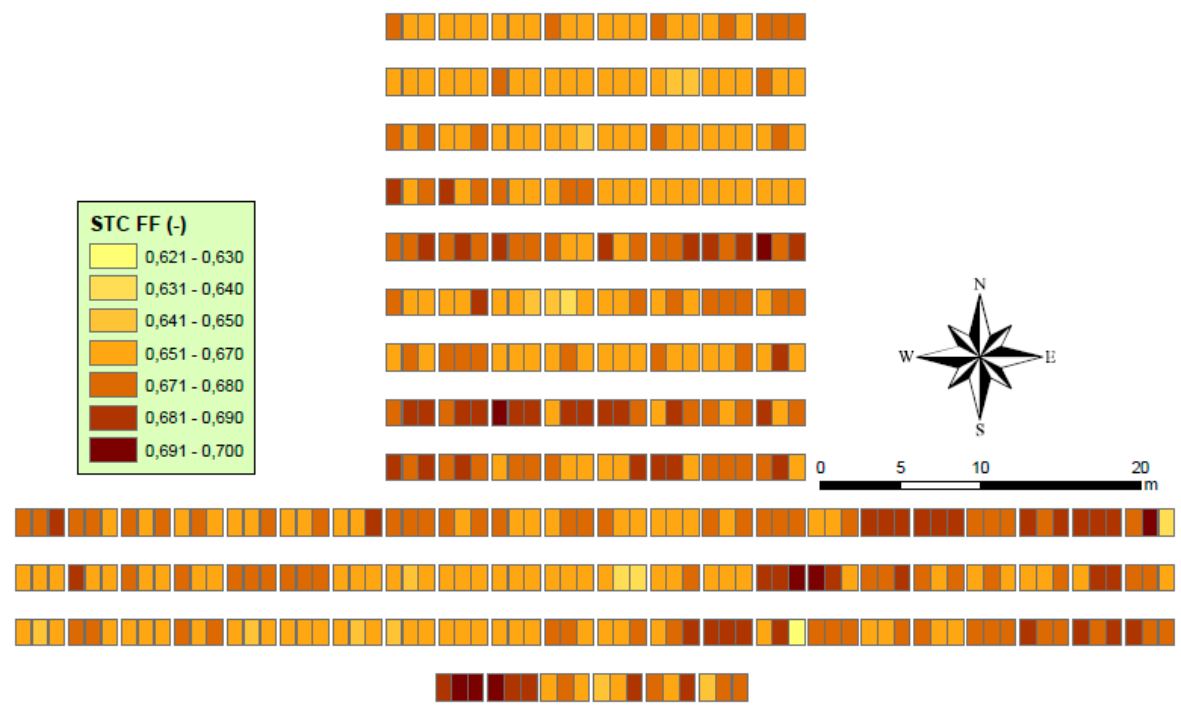**Figure 8 – STC peak power distribution analysis (108 kWp PV plant).**

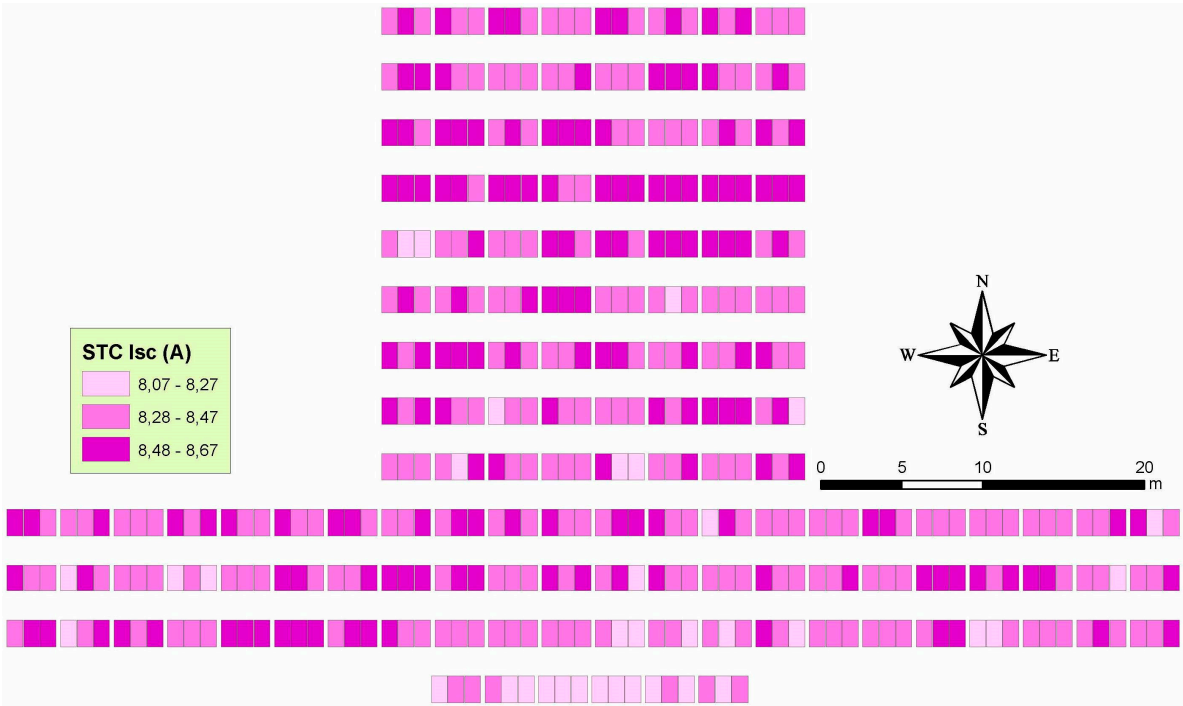**Figure 9 – STC fill factor distribution analysis (108 kWp PV plant).**

Figure 10 – STC short circuit current distribution analysis (108 kWp PV plant).
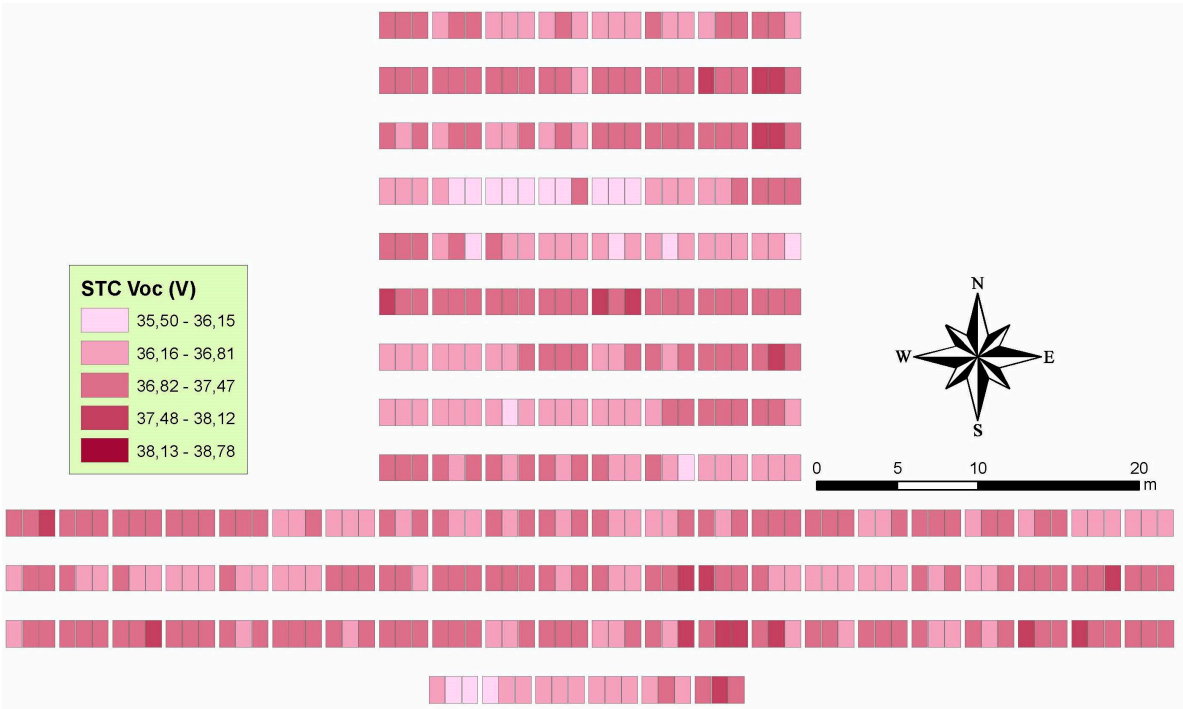

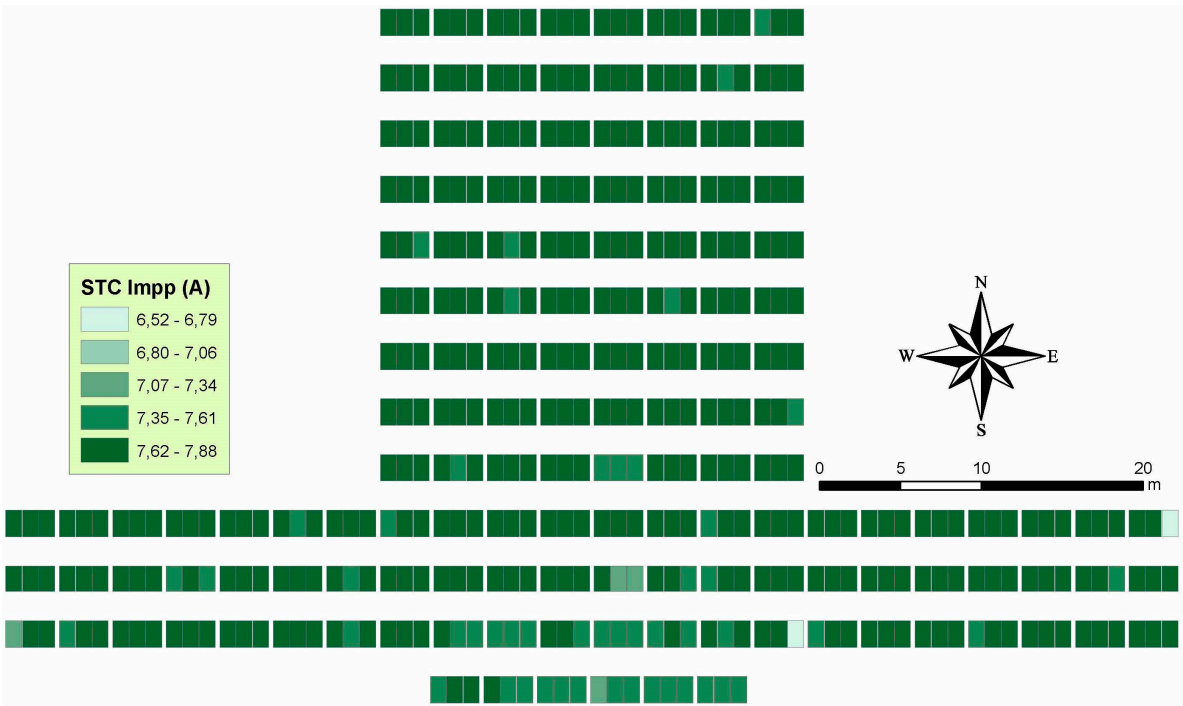**Figure 11 – STC open circuit voltage distribution analysis (108 kWp PV plant).**

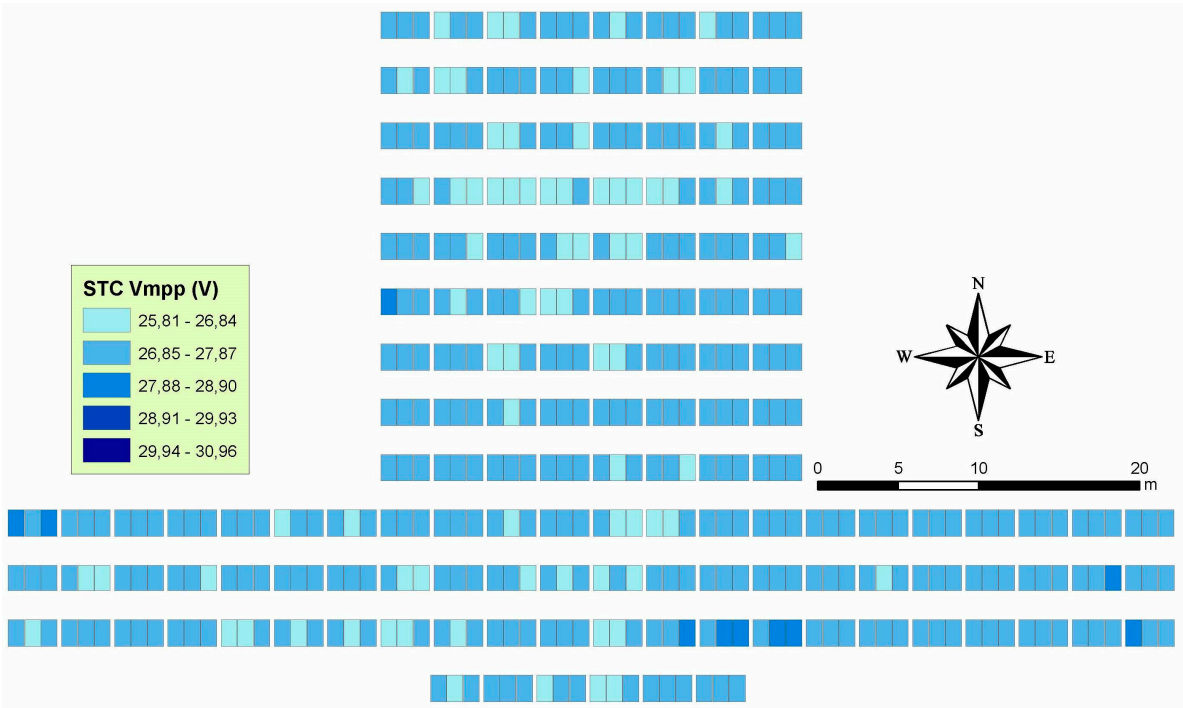**Figure 12 – STC maximum power current distribution analysis (108 kWp PV plant).**

Figure 13 – STC maximum power voltage distribution analysis (108 kWp PV plant).
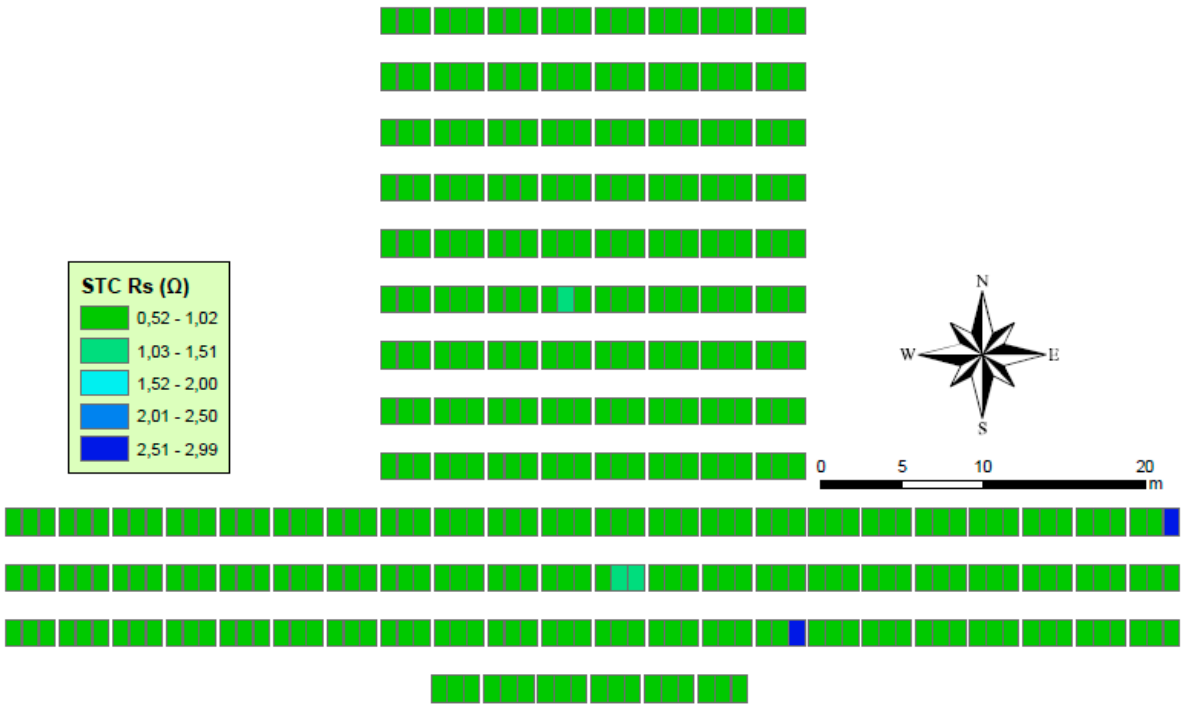
Figure 14 – Series resistance distribution analysis (108 kWp PV plant).
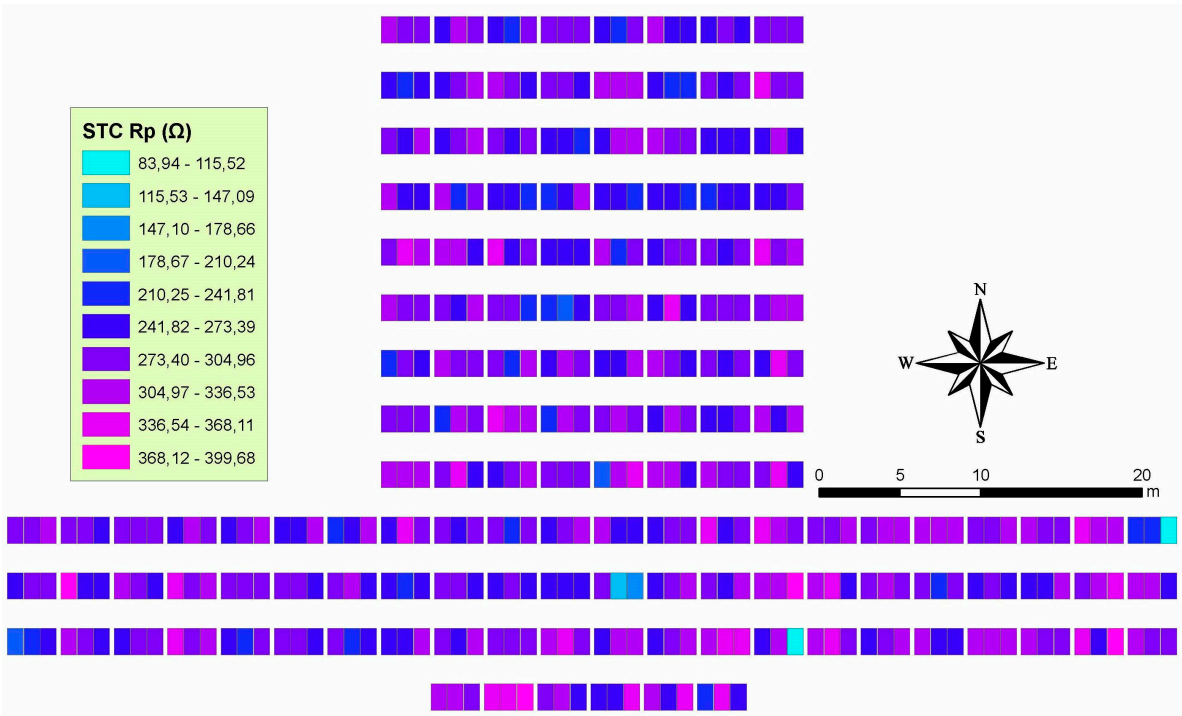
Figure 15 – Parallel resistance distribution analysis (108 kWp PV plant).
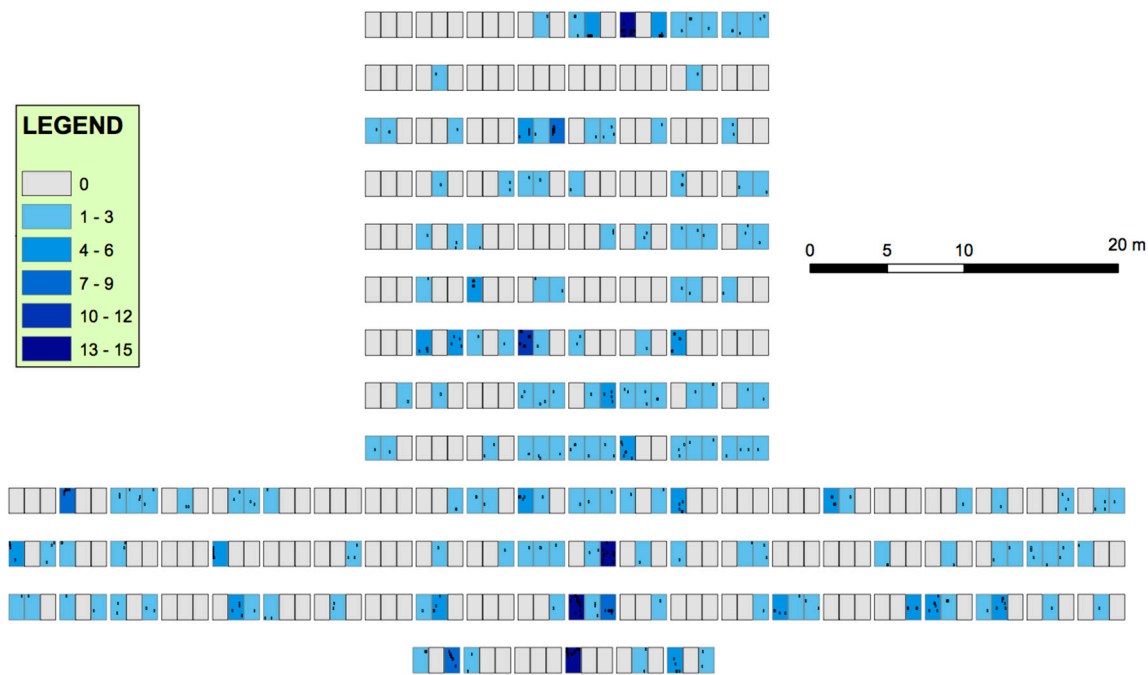
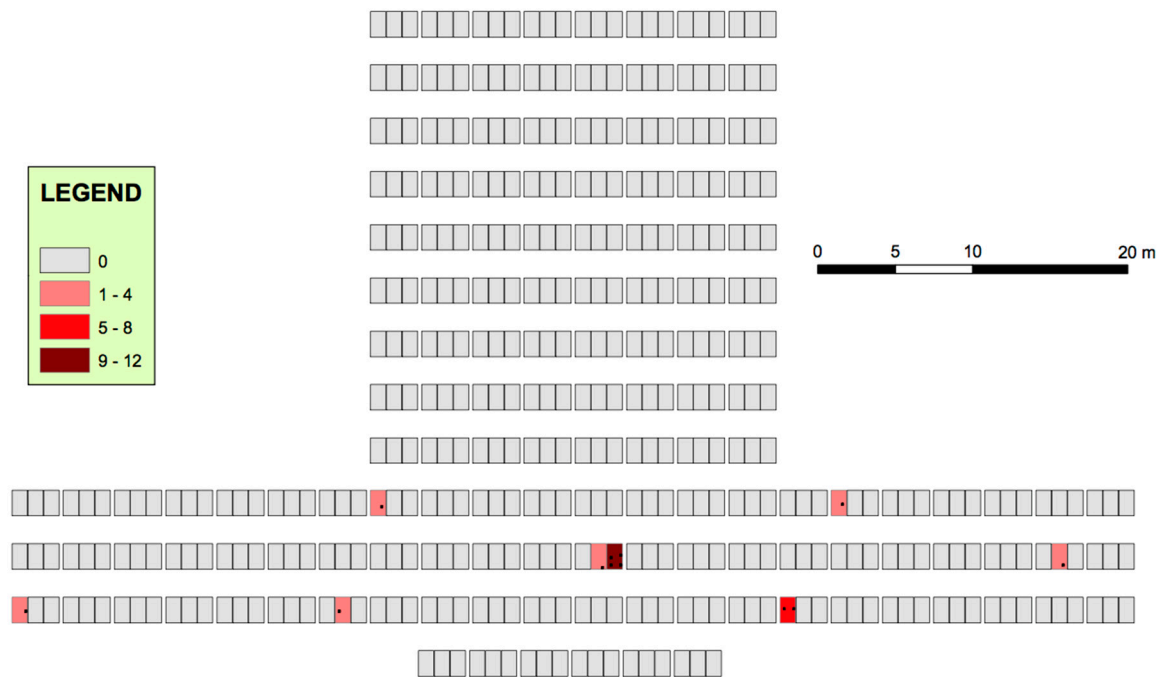**Figure 16 – Snail tracks distribution analysis (108 kWp PV plant).**

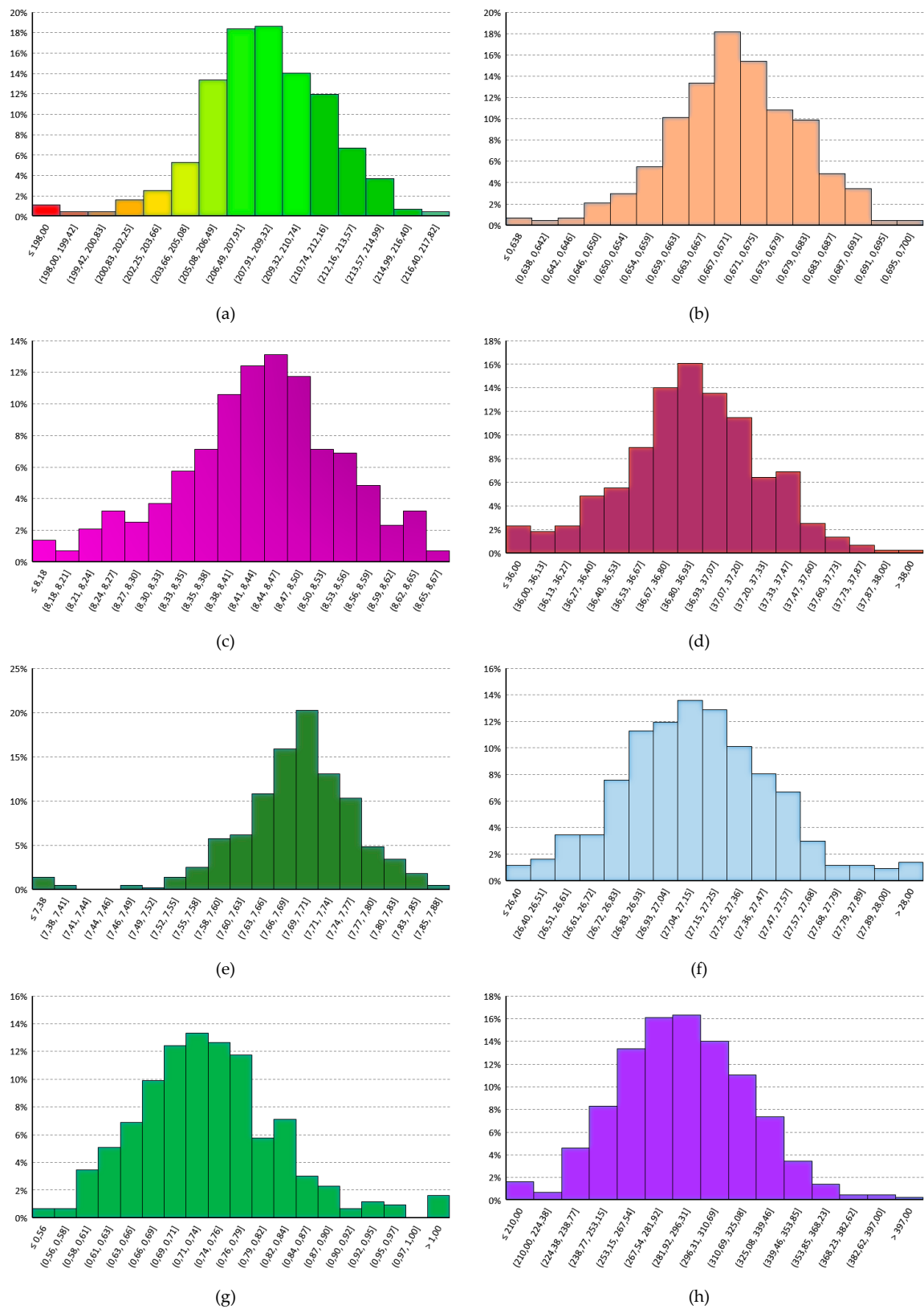**Figure 17 – Hot spots and burn marks distribution (108 kWp PV plant).**

Figure 18 – Histograms of the measured parameters in STC conditions for the 108 kWp PV plant: (a) peak power, (b) fill factor, (c) short circuit current, (d) open circuit voltage, (e) maximum power current, (f) maximum power voltage, (g) series resistance and (h) parallel resistance.

Table 4 – Found PV defects and associated average electrical parameters values.

	Snail tracks	Cell cracks	Hot spots and burn marks	Blue cells	Bubbles	Busbars discolorations	Cells discolorations	EVA discolorations
# Defects	418	9	36	540	3	4863	4140	40
# Modules	173	4	8	3	2	28	23	4
STC Peak Power [W]	207.93	207.17	203.59	205.78	207.12	206.73	208.91	207.38
STC I_{mpp} [A]	7.67	7.65	7.48	7.55	7.63	7.63	7.69	7.66
STC V_{mpp} [V]	27.13	27.06	27.20	27.24	27.15	27.08	27.15	27.07
STC I_{sc} [A]	8.43	8.40	8.38	8.18	8.32	8.38	8.43	8.45
STC V_{oc} [V]	36.85	36.73	36.77	36.96	36.52	36.86	36.85	37.06
R_s [Ohm]	0.77	0.73	0.90	0.67	0.65	0.75	0.72	0.81
R_p [Ohm]	282.92	291.49	238.00	355.32	312.36	289.61	293.70	271.81
FF (%)	0.67	0.67	0.66	0.68	0.68	0.67	0.67	0.66

Table 5 – Found PV defects correlations. Upper mid (above the main diagonal) is referred to the number of found defects while the lower mid (below the main diagonal) is referred to the number of modules.

	Snail tracks	Cell cracks	Hot spots and burn marks	Blue cells	Bubbles	Busbars discolorations	Cells discolorations	EVA discolorations
Snail tracks	418 / 173	0	7	0	0	42	18	0
Cell cracks	0	9 / 4	5	0	0	0	6	0
Hot spots and burn marks	2	2	36 / 8	0	0	12	6	0
Blue cells	0	0	0	540 / 3	0	0	0	0
Bubbles	0	0	0	0	3 / 2	0	1	0
Busbars discolorations	10	0	1	0	0	4863 / 28	180	0
Cells discolorations	8	2	2	0	1	1	4140 / 23	0
EVA discolorations	0	0	0	0	0	0	0	40 / 4

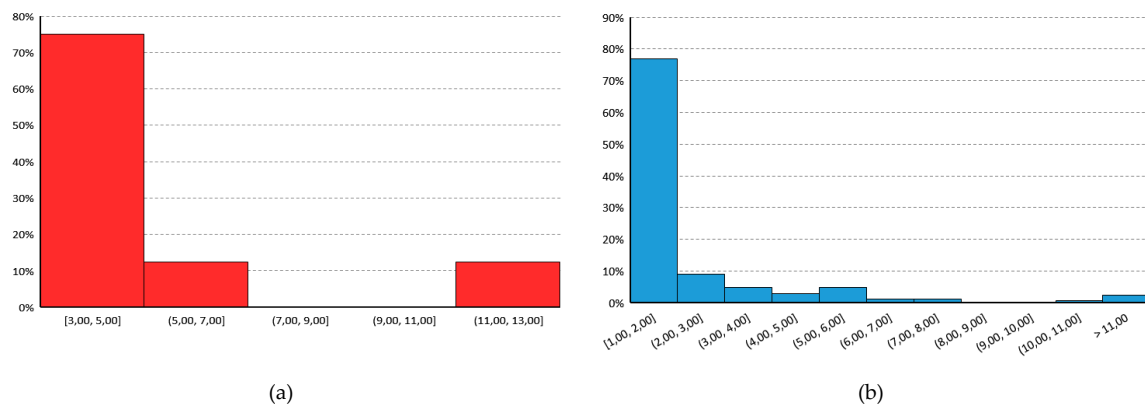(a)   (b)

Figure 19 – Histograms of the main PV faults found at the 108 kWp PV plant: (a) hot spots and burn marks and (b) snail tracks.

Table 6 – Degradation analysis on the 108 kWp PV plant. Variation of the measured values with respect to the nominal ones. Results expressed in %.

	Unharmed	Snail tracks	Cell cracks	Hot spots and burn marks	Blue cells	Bubbles	Busbars discolorations	Cells discolorations	EVA discolorations	Weighted average
Peak Power	-16.49	-16.83	-17.13	-18.56	-17.69	-17.15	-17.31	-16.44	-17.05	-16.72
I_{mpp}	-3.31	-3.64	-3.89	-6.03	-5.15	-4.15	-4.15	-3.39	-3.77	-3.56
V_{mpp}	-13.61	-13.60	-13.82	-13.38	-13.25	-13.54	-13.76	-13.54	-13.79	-13.61
I_{sc}	0.77	0.60	0.24	0.00	-2.39	-0.72	0.00	0.60	0.84	0.61
V_{oc}	-0.79	-0.94	-1.26	-1.16	-0.65	-1.83	-0.91	-0.94	-0.38	-0.87
R_s	168.86	181.11	166.51	228.58	144.61	137.30	173.81	162.86	195.72	174.38
R_p	-42.77	-43.83	-42.13	-52.75	-29.46	-37.99	-42.51	-41.69	-46.04	-43.19
FF	-16.44	-16.44	-16.44	-17.69	-15.19	-15.19	-16.44	-16.44	-17.69	-16.46

The developed GIS tool allows the analysis of the spatial PV degradation and defects location in an easier way than a traditional statistical analysis. Figure 18 shows the histograms of the measured parameters transformed to STC conditions.

Figure 8 shows lower peak power values for STC conditions in the center of the lower part of the installation, whereas the extremes show significantly higher values. This effect may be caused by the temperature distribution through the PV modules and the refrigeration by air convection conditions. The lowest STC peak power was 184.46 W, where the highest value was 217.82 W (18.09% difference). Sub-figure 18.a shows the distribution of the peak power values, where it can be noticed that more than the 70% of the modules are in the 205-211 Wp range.

In a similar way, figure 9 shows the fill factor of the PV modules transformed to the reference STC. Sub-figure 18.b shows the histogram for these values. It can be noticed that the PV modules are affected by a significant rate of degradation where 80% of the modules are in the range 0.66-0.68, when the nominal FF given by the manufacturer achieves 0.8018 (see table 3). Less than 1% of the PV modules present a FF>0.695. Moreover, it can be observed that those modules with lower values for peak power in figure 8 show also lower values of FF in figure 9. However, higher variations of the FF can be noticed in this late figure rather than on the peak power analysis. The fill factor distribution shows not to be homogeneous in the installation and, thus, modules with high values of fill factor

(FF) are linked to modules with very low values for FF. Some cases show differences up to 10.53%. This may affect significantly to the overall performance of the string series.

Figures 10 and 11 show the STC short circuit current and STC open circuit voltage distributions respectively. Moreover, Sub-figures 18.c and 18.d show their histograms. From that figures it can be observed that there exist very slight variations on the short circuit distribution (0.6 A max), but significant variations (up to 3.28 V) in the open circuit voltages. Both distributions in the spatial field are absolutely not homogeneous.

Figure 12 shows a uniform distribution of the STC maximum power current distribution apart from few PV modules which show current values in the range 6.52-6.79 A, while the average, according to sub-figure 18.e is 7.67 A, which is a 3.56% lower than the nominal I_{mpp}.

Figure 13 shows the STC maximum power voltage distribution. In this case, the distribution seems to be less homogeneous than the one seen for the maximum power current. Lowest maximum power voltage modules, in the range 25.81-26.84 are located in the northern and center parts of the PV plant, while certain modules located in the second row from the South show a higher voltage value. Histogram for this parameter, which can be seen in sub-figure 18.f shows a distribution close to the normal. with less than 4% of the voltage values higher than 27.68 V and less than 3% of the values lower than 26.40 V.

In Figure 12 it can be easily distinguished groups of PV modules with high values for the STC maximum power current. Distribution on the PV field of this electrical value is not uniform and low values can be correlated with low values of the STC maximum power voltage in Figure 13. Undoubtedly, those PV panels must be inspected with caution. Let's notice that higher differences on this value between close located PV modules can be found than when analyzing the maximum power voltage distribution.

Figures 14 and 15 show the distributions of the series resistance and parallel resistance of the PV modules respectively. Although both distributions are not the same, extreme values are located on the same PV modules. As it can be verified in Figure 15, these modules which have high values of series resistance and abnormally low values of parallel resistance, also present a significant high number of hot spots and burn marks (between 1 and 8). Moreover, according to Figure 8, those modules have very low power output. Thus, the whole string series production is affected. These PV panels must be replaced immediately. Fortunately, the rest of the series seem not to have been affected seriously. Sub-figures 18.g and 18.h show the histograms for both electrical parameters. The average for the series resistance is 0.7515 Ohm, while for the parallel resistance is 286.1831 Ohm. Both values are significantly different (higher in the case of the series resistance and lower for the parallel resistance) from the nominal ones, conducting to a considerable degradation rate.

Figures 16 and 17 include the most relevant PV defects on the installation: snail tracks and hot spots and burn marks. The snail tracks distribution in the power field seems not to be homogeneous but we cannot also infer a clear high density zone. PV modules affected by this PV fault seem to have from 1 to 3 defects. However, 15 defects of this type can be found on single modules. No significant correlations with electrical measurements are detected in this case.

Figure 17 show the hot spots and burn marks found on the PV modules. Fortunately, very few of these defects have been found in the installation. In this case, its distribution is clearly concentrated in the lowest part. Moreover, it results remarkable that the module with the highest number of hot spots and burn marks is also one with the highest number of snail tracks. Its STC peak power output is also lower than the average.

By analyzing Figures 8 and 16, it is observed that snail tracks may affect substantially to the power generation. Some modules with a high number of snail tracks show lower peak power values on STC. However, the thermographies did not detect significant variations on the PV module performance.

The rest of the defects are almost negligible in the power plant. Thus, no GIS tool images have been included but summary Tables 4 and 5 include them.

Table 4 shows the average values of the measured electrical parameters for each defect. On the other hand, Table 5 shows the correlations between found defects. This latter table is organized in

such a way it provides two values of interest. The upper mid above the main diagonal includes the counts of the cell parts affected simultaneously by two defects, while the lower mid below the main diagonal includes the counts of modules with both defects. Thus, it can be observed if in a module affected by several defects (lower mid) they appear in the same PV cell part or they are distributed among the module.

Table 4 shows that the lowest average STC peak power is associated with those modules affected by busbars discolorations, provoked by both significant diminutions of the maximum power current but not on the maximum power voltage. The series resistance and the parallel resistance also seems to be significantly affected in this case, but very few differences can be observed for the FF in comparison with the rest of PV modules defects.

PV faults correlations are shown in Table 5. The results show very few correlations between defects. However, it can be observed a high number of snail tracks produced on the same third cell than busbars discolorations and cells discolorations. These results also show a strong relationship between hot spots and burn marks with busbars and cells discolorations. PV modules affected by hot spots and burn marks also show a certain correlation with snail tracks and cell cracks.

Figure 19 shows both histograms for the hot spots and burn marks (a) and for the snail tracks (b) found in the power plant. Both histograms are expressed in relative terms to the modules affected by the considered fault. PV modules affected by hot spots and burn marks, near the 80% show between 3 and 5 faults simultaneously. The other 20% of damaged modules have a greater number of faults with a maximum record of 13 hot spots on a single module. On the other hand, sub-figure 18.b shows that utmost the 80% of the PV modules affected by the snail track fault have no more than two faults. Less than 1% of the PV modules damaged this way show more than 11 faults.

Finally, Table 6 summarizes the observed degradation on the 108 kWp PV plant by the variation of the measured electrical parameters with respect to the nominal ones. The weighted average degradation of the peak power is close to the 17% meaning an average linear degradation rate of 1.86%/year. Unharmed PV modules show a lower degradation rate of 16.49%, while the higher degradation is shown on those PV modules affected by hot spots and burn marks (18.56%). Found variations on short circuit current and open circuit voltage are almost negligible, but significant worsening on the series and parallel resistance values are observed.

4.2. *Implementation on a 9 kWp PV power plant*

The second case study is a self-consumption PV power plant operated by the Spanish company Himalaya Sol. It is a fixed 9 kWp plant installed in the rooftop of a single family dwelling. It started the operation in February 2017 and consists of 36 *GFM 220-250* monocrystalline silicon modules manufactured by the company *Wuxi Guofei Green Energy Source Co. Ltd*. (see Table 3). The PV modules are installed in a fixed structure with a slope of 32 degrees and oriented 6 degrees East azimuth angle. The modules have a unit peak power of 250 W and its power output is optimized by a *P300* optimizer from *Solar Edge*, as the installation is affected by a high number of shadows (due to the architectural configuration).

The PV modules are organized in 3 series strings which consists of two strings of 13 modules and one string of 10 modules. The power output from each string is transformed from DC to AC by a 3 kW nominal power inverter manufactured by Solar Edge. Each inverter includes the necessary protections.

As the energy injection to the power grid is not allowed in this installation (it has been regularized as Type 1 self-consumption facility according to [41]) a relay regulates and/or disconnects the power plant in case the consumption gets lower than the power output.

Due to the novelty of the installation, only the preliminary analysis has been carried out in this case. Thus, only the initial modules test and the geodatabase generation have been done.
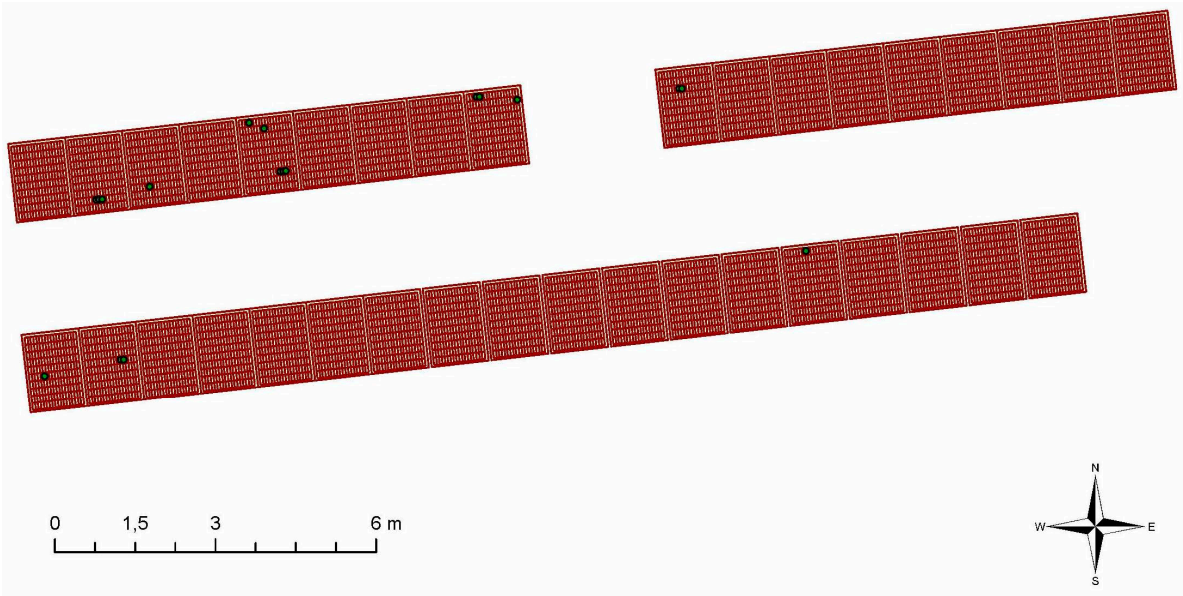
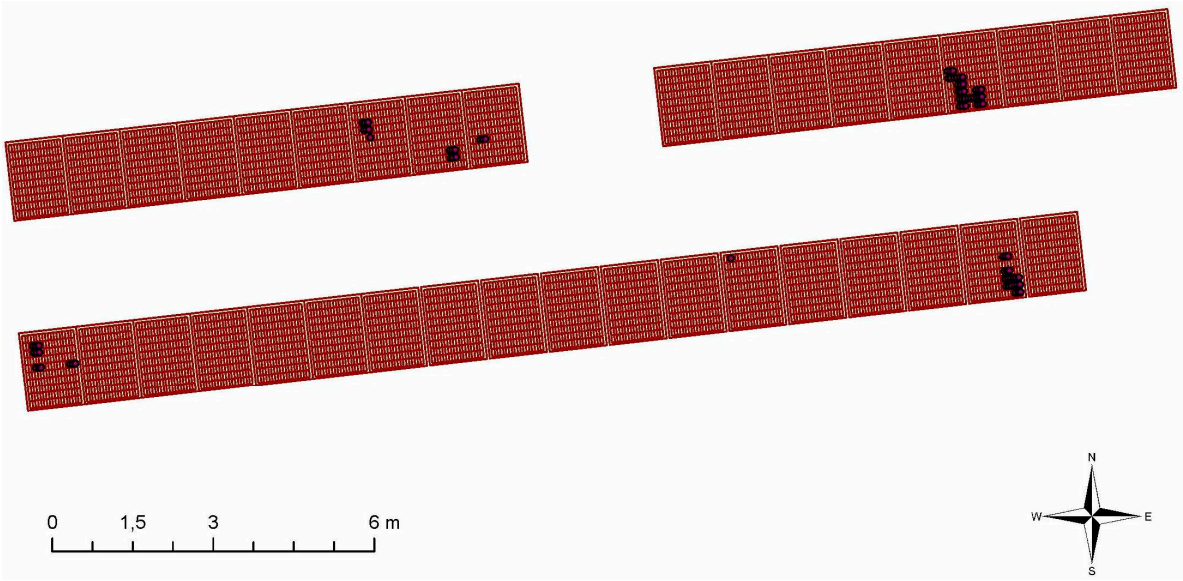**Figure 20 – Snail tracks distribution (9 kWp PV plant).**

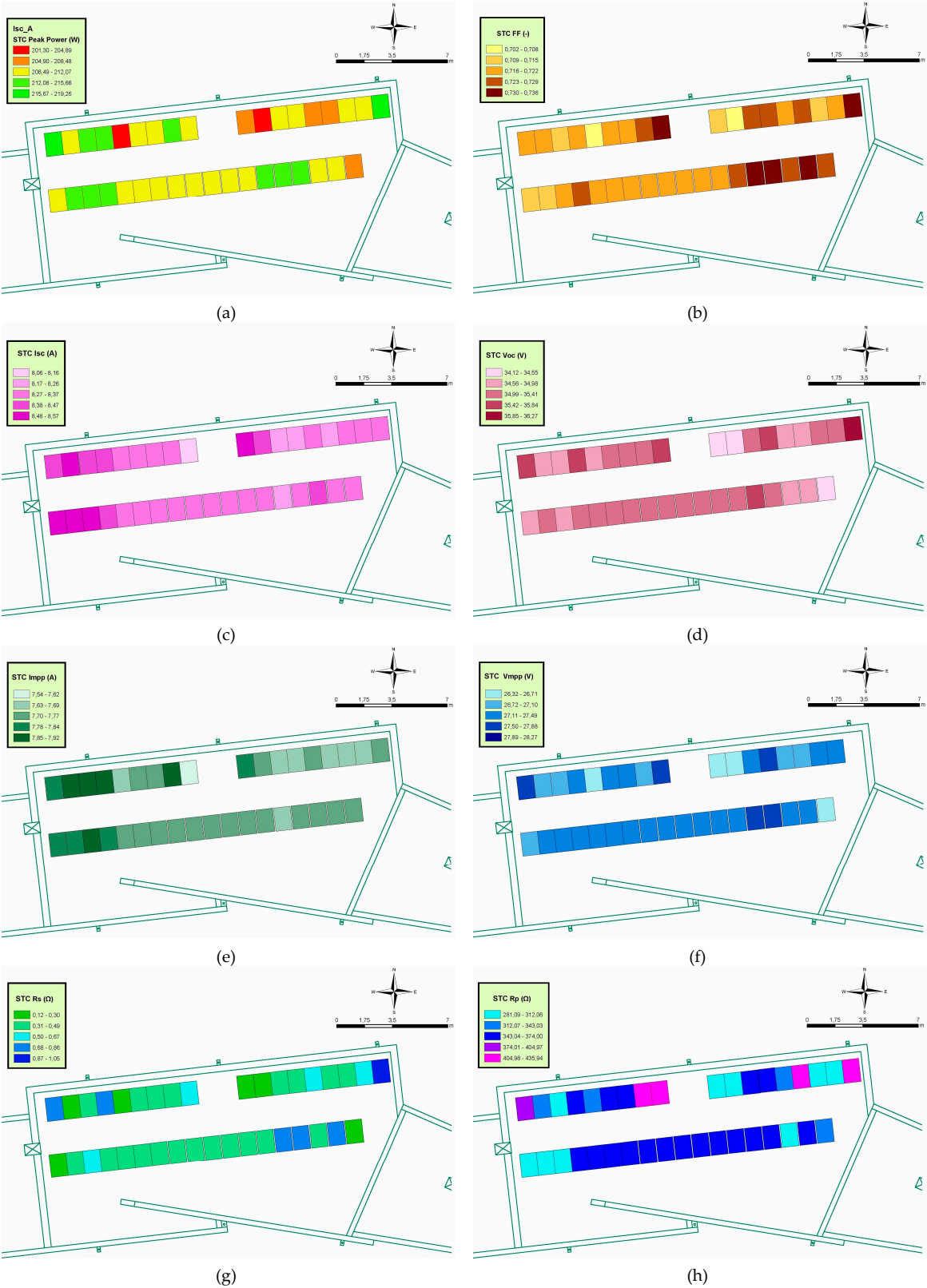**Figure 21 – Cells discoloration distribution (9 kWp PV plant).**

Figure 22 – Electrical parameters in STC conditions distributions: (a) peak power, (b) fill factor (c) short circuit current, (d) open circuit voltage, (e) maximum power current, (f) maximum power voltage, (g) series resistance, (h) parallel resistance (9 kWp PV plant).
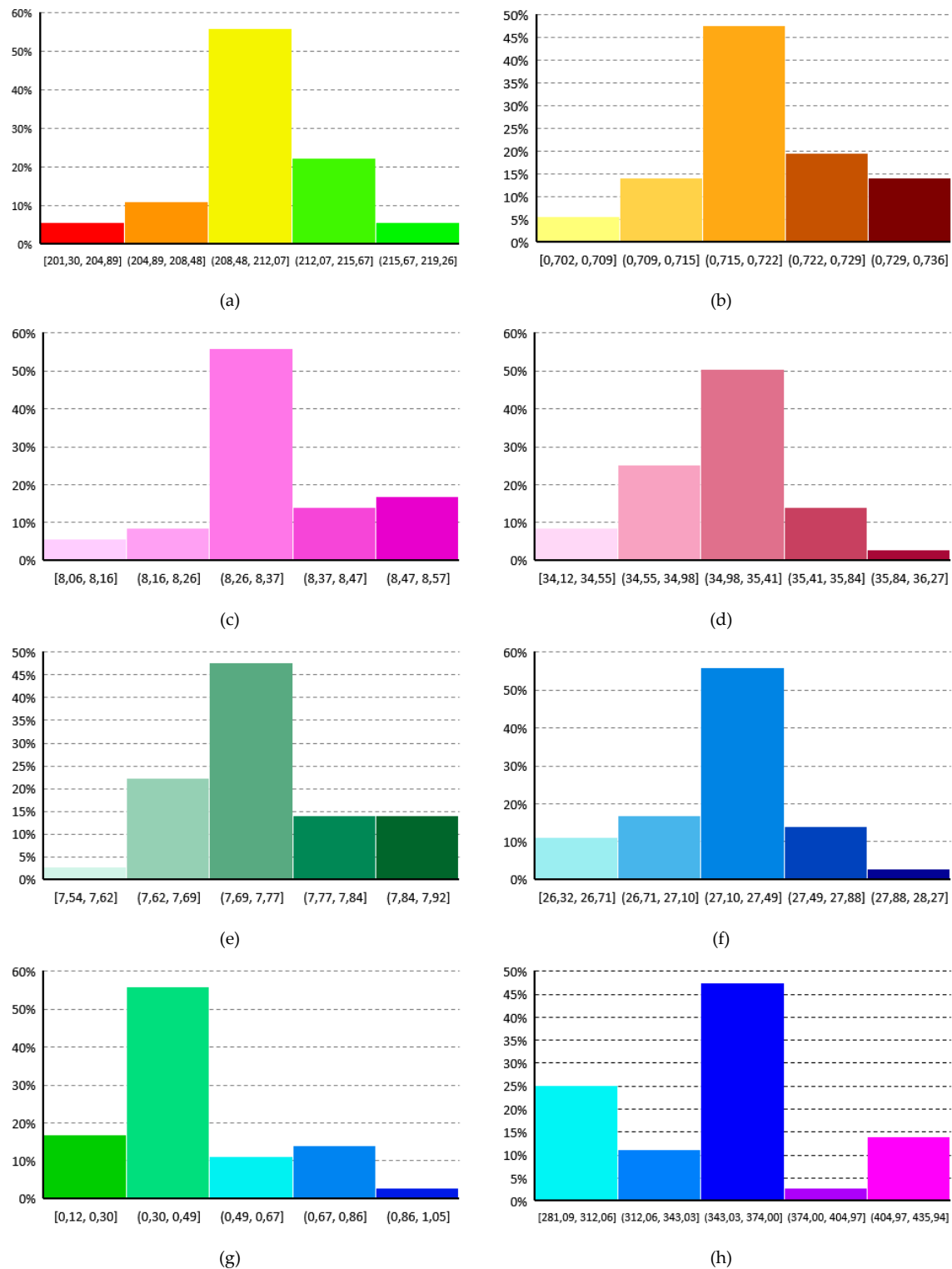
Figure 23 – Histograms of the measured parameters in STC conditions for the 9 kWp PV plant: (a) peak power, (b) fill factor, (c) short circuit current, (d) open circuit voltage, (e) maximum power current, (f) maximum power voltage, (g) series resistance and (h) parallel resistance.

Table 7 – Found PV defects and associated average electrical parameters values.

	Snail tracks	Blue cells	Busbars discolorations	Cells discolorations
# Defects	18	36	1	83
# Modules	8	3	1	7
STC Peak Power [W]	210.04	212.30	209.63	209.80
STC I_{mpp} [A]	7.77	7.78	7.65	7.71
STC V_{mpp} [V]	27.02	27.30	27.40	27.20
STC I_{sc} [A]	8.41	8.36	8.35	8.28
STC V_{oc} [V]	34.91	35.15	35.23	34.97
R_s [Ohm]	0.34	0.61	0.48	0.42
R_p [Ohm]	323.02	356.90	283.85	368.37
FF (%)	72.00%	72.00%	71.26%	72.00%

Table 8 – Found PV defects correlations. Upper mid (above the main diagonal) is referred to the number of found defects while the lower mid (below the main diagonal) is referred to the number of modules.

	Snail tracks	Blue cells	Busbars discolorations	Cells discolorations
Snail tracks	18 / 8	0	0	0
Blue cells	0	36 / 3	0	0
Busbars discolorations	0	0	1 / 1	0
Cells discolorations	2	0	0	83 / 7

Table 9 – Degradation analysis on the 9 kWp PV plant. Variation of the measured values with respect to the nominal ones. Results expressed in %.

	Unharmed	Snail tracks	Blue cells	Busbars discolorations	Cells discolorations	Weighted average
Peak Power	-15.50	-15.98	-15.08	-16.15	-16.08	-15.69
I_{mpp}	-2.69	-2.39	-2.26	-3.89	-3.14	-2.71
V_{mpp}	-13.14	-13.95	-13.06	-12.74	-13.38	-13.34
I_{sc}	-0.47	0.36	-0.24	-0.36	-1.19	-0.41
V_{oc}	-5.65	-6.16	-5.51	-5.30	-5.99	-5.80
R_s	81.86	24.13	122.70	75.24	53.34	67.50
R_p	-30.96	-35.87	-29.15	-43.65	-26.87	-31.43
FF	-10.00	-10.20	-10.20	-11.12	-10.20	-10.12

A similar analysis to the previous one can be conducted in this case. However, results for the implementation in the 9 kWp PV power plant have not much relevance yet. As the installation started working recently almost no degradation has still been observed. However, Figures 20 and 21 show several snail tracks and cells discolorations that may conduct to a more detailed maintenance needs on these modules. Distributions of both defects are clearly not homogeneous and they look to concentrate on the string series extremes.

Figure 22 shows the electrical measures distributions for the second case study. The distributions in all cases are more homogeneous than in the previous case study due to the lower rate of degradation. In this case, major variations are found for maximum power current 22.c, short circuit current 22.f and parallel resistance 22.h. Actually, a correlation between low values of short circuit values and cell discolorations can be found in this case.

Tables 7 and 8 show the results for the 9 kWp PV plant. In this case, only four defects have been found: snail tracks, blue cells, busbars discolorations and cells discolorations. Relative apparition rates are not similar than in the previous case study. This fact leads to think in a spatially and temporally spread process. It can be also observed that, in this case, the impact of the blue cells defect on the STC peak power is much lower than in the previous case. Moreover, although both installations have similar fill factor values for the PV modules, in the second case, higher maximum power current values have been measured than in the first case, but lower maximum power voltages.

Parallel resistances are higher in the second installation than in the first one for all classified defects, but for the busbars discoloration fault. On the other hand, series resistance values are significantly lower than in the first case, but for the blue cells fault, which is found to be similar.

Figure 23 shows the histograms for the measured electrical parameters for this case study. In this case, dispersions of the values are lower than for the 108 kWp power plant and, thus, fewer bins are identified. Subfigure 23.a shows that the average STC peak power is 210.77 Wp and less than 5% of the modules have less than 204.89 Wp. On the other hand, fill factor for the PV modules installed in this plant have a higher value, closer to the nominal one. 80% of the PV modules have a fill factor in the range between 71% and 73%.

Sub-figures 23.c-f show the histograms for I_{sc}, V_{oc}, I_{mpp} and V_{mpp}, respectively. Dispersion of these parameters is too low and no high differences with the nominal values are observed.

Finally, sub-figures 23.g and 23.h show the histograms for the series and parallel resistances. 55% of the modules have a series resistance in the range between 0.30 and 0.49 ohms, while for the parallel resistance, 47% are in the range between 343 and 374 ohms, but a significant 25% of the modules have a parallel resistance lower than 312 ohms.

Table 8 shows the correlations between PV defects in the second case and it is organized in the same way as Table 5. In this case, only two modules presented both snail tracks and cells discolorations. This result is in accordance with the obtained in the first installation where a high number of PV modules affected by cells discolorations also presented snail tracks defects.

Finally, Table 9 summarizes the observed degradation on the 9 kWp PV plant by the variation of the measured electrical parameters with respect to the nominal ones. The weighted average degradation of the peak power is close to the 15.7%. Unharmed PV modules show a lower degradation rate of 15.50%, while the higher degradation is shown on those PV modules affected by cells discolorations (16.08%). Found variations on short circuit current and open circuit voltage are almost negligible, but significant worsening on the series and parallel resistance values are observed.

5. Conclusions

The designed GIS tool has proven to be useful to analyze the degradation effects on a PV field and the most common PV defects location and correlation. Although its implementation has proportioned useful information for both cases study, its application to big plants seems to be more feasible that for small installations.

The results show no straight correlations between PV defects, snail tracks and cell cracks with different types of discolorations. On the other hand, the electrical parameters on the modules seems

not to be uniformly distributed in the power plant and no correlations with defects can be found apart from blue cells, which initially was not considered a relevant defect.

For both cases study the GIS tool has been proved to be helpful to analyze the degradation rates of the PV modules. Moreover, in contrast with other analyzing techniques, the proposed methodology includes information on the spatial distribution of the PV faults, allowing, in future research, to evaluate the impact of mismatching PV modules affected by faults with unharmed ones.

The presented GIS tool will become really useful to supervise the electrical parameters degradation in the power plant and the defects evolution and distribution in the PV field. Researchers and maintenance service are encouraged to apply this tool to their installations and compare the results. In our case, periodical measurements and inspections will be added to the geodatabase and the real degradation of the PV field will be then deeply analyzed. This will conduct to more effective preventive maintenance actuations as well as a more economic modules replacement strategies.

Conflicts of Interest: The authors declare no conflict of interest.

References

1. Woyte, A.; Goy, S. 11 - Large grid-connected photovoltaic power plants: Best practices for the design and operation of large photovoltaic power plants. In *The Performance of Photovoltaic (PV) Systems*; Pearsall, N., Ed.; Woodhead Publishing, 2017; pp. 321–337.

2. Ventura, C.; Tina, G. M. Utility scale photovoltaic plant indices and models for on-line monitoring and fault detection purposes. *Electr. Power Syst. Res.* **2016**, *136*, 43–56.

3. Bizzarri, F.; Brambilla, A.; Caretta, L.; Guardiani, C. Monitoring performance and efficiency of photovoltaic parks. *Renew. Energy* **2015**, *78*, 314–321.

4. Shariff, F.; Rahim, N. A.; Hew, W. P. Zigbee-based data acquisition system for online monitoring of grid-connected photovoltaic system. *Expert Syst. Appl.* **2015**, *42*, 1730–1742.

5. Hohn, J.; Lehtonen, E.; Rasi, S.; Rintala, J. A Geographical Information System (GIS) based methodology for determination of potential biomasses and sites for biogas plants in southern Finland. *Appl. Energy* **2014**, *113*, 1–10.

6. Gastli, A.; Charabi, Y. Solar electricity prospects in Oman using GIS-based solar radiation maps. *Renew. Sustain. Energy Rev.* **2010**, *14*, 790–797.

7. Kakumoto, Y.; Koyamatsu, Y.; Shiota, A.; Qudaih, Y.; Mitani, Y. Application of Geographic Information System to Power Distribution System Analysis. In; 2016; Vol. 100, pp. 360–365.

8. Tsanakas, J. A.; Ha, L. D.; Al, S. Advanced inspection of photovoltaic installations by aerial triangulation and terrestrial georeferencing of thermal/visual imagery. *Renew. Energy* **2017**, *102*, 224–233.

9. Shiota, A.; Fuchino, G.; Koyamatsu, Y.; Kakumoto, Y.; Tanoe, K.; Qudaih, Y.; Mitani, Y. Guide Construction of an Efficient Inspection, Maintenance and Asset Management of Photovoltaic Power Generation System using GIS. *Energy Procedia* **2016**, *100*, 69–77.

10. Köntges M.; Kurtz S.; Packard C.; Jahn U.; Berger K.A.; Kato, K.; Friesen T.; Liu H.; Van Iseghem M. IEA-PVPS T13-01 2014 Review of Failures of PV Modules Final.

11. Urra Medina, E.; Barría Pailaquilén, R. M. La revisión sistemática y su relación con la práctica basada en la evidencia de la salud. *Rev Lat.-Am* **2010**, *18*, 1–8.

12. Meade, M. O.; Richardson, W. S. Selecting and appraising studies for a systematic review. *Ann. Intern. Med.* **1997**, *127*, 531–537.

13. Jansen, K. W.; Delahoy, A. E. A laboratory technique for the evaluation of electrochemical transparent conductive oxide delamination from glass substrates. *Thin Solid Films* **2003**, *423*, 153–160.

14. Veldman, D.; Bennett, I. J.; Brockholz, B.; Jong, P. C. de Non-destructive testing of crystalline silicon photovoltaic back-contact modules. In *2011 37th IEEE Photovoltaic Specialists Conference*; 2011; pp. 003237–003240.

15. Knausz, M.; Oreski, G.; Eder, G. C.; Voronko, Y.; Duscher, B.; Koch, T.; Pinter, G.; Berger, K. A. Degradation of photovoltaic backsheets: Comparison of the aging induced changes on module and component level. *J. Appl. Polym. Sci.* **2015**, *132*, n/a-n/a.

16. Trout, T. J.; Hu, H.; Wang, C. F.; Garreau-Iles, L.; Heta, Y.; Stika, K. M.; Yu, B.-L.; Hamzavy, B.; Bradley, A.; MacMaster, S.; Felder, T.; Kopchick, J.; Gambogi, W. Backsheet Designs Critical to PV Module Performance, Safety and Durability. *31st Eur. Photovolt. Sol. Energy Conf. Exhib.* **2015**, 1930–1934.

17. Jordan, D. C.; Kurtz, S. R. Photovoltaic Degradation Rates—an Analytical Review. *Prog. Photovolt. Res. Appl.* **2013**, *21*, 12–29.

18. Montserrat, D. M.; Saldaña-Mayor D.; Dieste-Velasco M.I.; González-Peña D.; Alonso-Tristán C. Degradation in silicon PV modules: fault distribution analysis in grid connected facilities over long period of operation. In; Amsterdam, Niederlande, 2014.

19. Kajari-Schröder, S.; Kunze, I.; Eitner, U.; Köntges, M. Spatial and orientational distribution of cracks in crystalline photovoltaic modules generated by mechanical load tests. *Sol. Energy Mater. Sol. Cells* **2011**, *95*, 3054–3059.

20. Sander, M.; Dietrich, S.; Pander, M.; Schweizer, S.; Ebert, M.; Bagdahn, J. Investigations on crack development and crack growth in embedded solar cells. In; 2011; Vol. 8112, pp. 811209-811209–10.

21. Köntges, M.; Kunze, I.; Kajari-Schrder, S.; Breitenmoser, X.; Bjørneklett, B. The risk of power loss in crystalline silicon based photovoltaic modules due to micro-cracks. *Sol. Energy Mater. Sol. Cells* **2011**, *95*, 1131–1137.

22. Struwe, R.; Wang, E.; Chi, S.; Huang, S. Y.; Chien, Y. C.; Shiu, S.-M.; Chou, W. Y.; Chou, Y. H. Chemical Analysis and Proposed Generating Mechanism for Snail Tracks Contamination of EVA Encapsulated Modules. *27th Eur. Photovolt. Sol. Energy Conf. Exhib.* **2012**, 3132–3136.

23. Dolara, A.; Leva, S.; Manzolini, G.; Ogliari, E. Investigation on performance decay on photovoltaic modules: Snail trails and cell microcracks. *IEEE J. Photovolt.* **2014**, *4*, 1204–1211.

24. Martinez Moreno, F. Caracterización y modelado de grandes centrales fotovoltaicas, Telecomunicacion, 2012.

25. Pingel, S.; Frank, O.; Winkler, M.; Daryan, S.; Geipel, T.; Hoehne, H.; Berghold, J. Potential Induced Degradation of solar cells and panels. In *2010 35th IEEE Photovoltaic Specialists Conference (PVSC)*; 2010; pp. 002817–002822.

26. Luo, W.; Khoo, Y. S.; Hacke, P.; Naumann, V.; Lausch, D.; Harvey, S. P.; Singh, J. P.; Chai, J.; Wang, Y.; Aberle, A. G.; Ramakrishna, S. Potential-induced degradation in photovoltaic modules: a critical review. *Energy Environ. Sci.* **2017**, *10*, 43–68.

27. Köntges, M. *Reviewing the practicality and utility of electroluminescence and thermography images*; PHOTOVOLTAIC POWER SYSTEMS PROGRAMME; Institute for Solar Energy Research Hamelin.

28. Green, M. A.; Hasyim, E. S.; Wenham, S. R.; Willison, M. R. SILICON SOLAR CELLS WITH INTEGRAL BYPASS DIODES. In; 1984; pp. 513–517.

29. Moldes Teo, F. J. *Tecnología de los Sistemas de Información Geográfica*; Rama: Madrid, 1995.

30. FIR Thermal imaging cameras: a fast and reliable tool for testing solar panels 2015.

31. FLIR *Thermal imaging guidebook for building and renewable energy applications.*; Infrared Training Center (ITC)., 2011.

32. López Meraz, R. A. Análisis térmico de las celdas fotovoltaicas en un sistema interconectado a la red., Veracruzana: Veracruz, 2012.

33. AENOR. Norma CEI 60904-1:2006 (accessed Mar 25, 2017).

34. Sansoni, P.; Fontani, D.; Francini, F.; Jafrancesco, D.; Pierucci, G.; De Lucia, M. Technique for Outdoor Test on Concentrating Photovoltaic Cells. *Int. J. Photoenergy Int. J. Photoenergy* **2015**, *2015*, *2015*, e308541.

35. Buerhop, C.; Schlegel, D.; Niess, M.; Vodermayer, C.; Weißmann, R.; Brabec, C. J. Reliability of IR-imaging of PV-plants under operating conditions. *Sol. Energy Mater. Sol. Cells* **2012**, *107*, 154–164.

36. Bendel, C.; Wagner, A. Photovoltaic measurement relevant to the energy yield. In *WCPEC-3 World Conference on Photovoltaic Energy Conversion*; Osaka, Japan, 2003; Vol. 7P–B3–09, pp. 1–4.

37. IEC *IEC 60891:2009 Edition 2.0 - Photovoltaic devices - Procedures for temperature and irradiance corrections to meausured I-V characteristics*; 2009.

38. Wagner, A. Peak-Power and internal series resistance measurement under natural ambient conditions. In *EuroSun 2000*; Copenhagen, 2000; pp. 1–7.

39. Trentadue, G.; Pavanello, D.; Salis, E.; Field, M.; Müllejans, H. Determination of internal series resistance of PV devices: Repeatability and uncertainty. *Meas. Sci. Technol.* **2016**, *27*, 055005 (9pp).

40. Green, M. A. Accurate expression for solar cell fill factors including series and shunt resistance. *Applait Phys. Lett.* **2016**, *108*, 081111-1–5.

41. MINISTERIO DE INDUSTRIA, ENERGÍA Y TURISMO *Real Decreto 900/2015, de 9 de octubre, por el que se regulan las condiciones administrativas, técnicas y económicas de las modalidades de suministro de energía eléctrica con autoconsumo y de producción con autoconsumo.*; 2015; Vol. Nº 243, pp. 94874–94917.